Geochimica et Cosmochimica Acta, Vol. 69, No. 1, pp. 63-81, 2005

0016-7037/05 $30.00 + .00

doi:10.1016/j.gca.2004.06.028

Surface complexation of neodymium at the rutile-water interface: A potentiometric and modeling study in NaCl media to 250°C

MOIRA K. RIDLEY,[1,*] MICHAEL L. MACHESKY,[2] DAVID J. WESOLOWSKI,[3] and DONALD A. PALMER[3]

[1]Texas Tech University, Department of Geosciences, P.O. Box 41053, Lubbock, TX 79409-1053, USA
[2]Illinois State Water Survey, 2204 Griffith Drive, Champaign, IL 61820-7495, USA
[3]Chemical Sciences Division, Oak Ridge National Laboratory, P.O. Box 2008, MS 6110, Oak Ridge, TN 37831-6110, USA

(*Received January* 15, 2004; *accepted in revised form June* 22, 2004)

Abstract—The adsorption of Nd^{3+} onto rutile surfaces was examined by potentiometric titration from 25 to 250°C, in 0.03 and 0.30*m* NaCl background electrolyte. Experimental results show that Nd^{3+} sorbs strongly, even at low temperature, with adsorption commencing below the pH_{znpc} of rutile. In addition, there is a systematic increase in Nd^{3+} adsorption with increasing temperature. The experimental results were rationalized and described using surface oxygen proton affinities computed from the MUlti SIte Complexation or MUSIC model, coupled with a Stern-based three-layer description of the oxide/water interface. Moreover, molecular-scale information was incorporated successfully into the surface complexation model, providing a unique geometry for the adsorption of Nd^{3+} on rutile. The primary mode of Nd^{3+} adsorption was assumed to be the tetradentate configuration found for Y^{3+} adsorption on the rutile (110) surface from previously described in situ X-ray standing wave experiments, wherein the sorbing cations bond directly with two adjacent "terminal" and two adjacent "bridging" surface oxygen atoms. Similarly, the adsorption of Na^+ counterions was also assumed to be tetradentate, as supported by MD simulations of Na^+ interactions with the rutile (110) surface, and by analogous X-ray standing wave results for Rb^+ adsorption on rutile. Fitting parameters for Nd^{3+} adsorption included binding constants for the tetradentate adsorption complex and capacitance values for the inner-sphere binding plane. In addition, hydrolysis of the tetradentate adsorption complex was permitted and resulted in significantly improved model fits at higher temperature and pH values. The modeling results indicate that the Stern-based MUSIC surface-complexation model adequately accommodates molecular-scale information to uniquely rationalize and describe multivalent ion adsorption systematically into the hydrothermal regime.

1. INTRODUCTION

The partitioning of ions and the disruption of bulk phase properties at the interface between minerals and aqueous solutions, a region commonly referred to as the Electric Double Layer (EDL), involves a complex interplay of chemical, electrostatic and crystallographic factors (Brown et al., 1999, and references therein). Conceptual descriptions of the EDL are provided by various surface complexation models (e.g., Westall and Hohl, 1980; Davis and Kent, 1990; Dzombak and Morel, 1990; Criscenti and Sverjensky, 2002) and are routinely used to rationalize and describe bulk-macroscopic experimental data. Traditionally, surface complexation models have been ambiguous, because experimental ion adsorption and electrokinetic data could not be fitted uniquely. Moreover, model parameter values (i.e., binding constants of hypothetical surface species and Stern Layer capacitance values) were often highly covariant. However, it is now possible to uniquely constrain macroscopic ion-adsorption data within surface complexation models that fully integrate molecular-scale and crystallographic information, providing conceptual models that are mechanistically accurate and thermodynamically rigorous (Hiemstra and van Riemsdijk, 2002).

The Multi Site Complexation (MUSIC) model, developed by Hiemstra et al. (1989, 1996), includes specific consideration of the proton affinities of the various types of surface oxygens known to exist on individual crystallographic faces exposed on mineral surfaces. In addition, this model can directly accommodate in situ molecular-scale information provided by X-ray techniques such as, in situ small-period X-ray standing waves (Bedzyk and Cheng, 2002; Fenter et al., 2000) and grazing-incidence X-ray absorption (GI-XAF) spectroscopy (Towle et al., 1999a,b; Waychunas, 2002). Several previous studies have demonstrated the ability of the MUSIC model to directly accommodate in situ spectroscopic information (e.g., Venema et al., 1996;Rietra et al., 2001; Boily, 1999). Most of these studies have utilized the "one-pK" model, which can be considered the simplest representation of the MUSIC model (Gibb and Koopal, 1990). Moreover, most of these studies were conducted at room temperature only. Recently, Ridley et al. (2004) modeled the adsorption of Ca^{2+} onto rutile using the temperature compensated MUSIC model (Machesky et al., 2001) approach, and incorporated the tetradentate, inner sphere, adsorption geometry found by Fenter et al. (2000) for Sr^{2+} adsorption on the rutile (110) surface. The study of Ridley et al. (2004) demonstrated that in situ spectroscopic and X-ray information that are necessary to uniquely describe ion adsorption to mineral surfaces can be directly and successfully accommodated within the MUSIC model over a wide temperature range (to at least 250°C).

In the present study, we continue our approach of modeling potentiometric adsorption data utilizing the MUSIC model (Hiemstra et al., 1989, 1996; Machesky et al., 2001) that

* Author to whom correspondence should be addressed (moira.ridley@ttu.edu).

incorporates unique ion adsorption configurations from X-ray information, to rationalize and describe the adsorption of a trivalent cation, Nd^{3+}, onto the surface of rutile. Interest in Nd^{3+} was stimulated by its chemical similarity to trivalent actinides, and the need to understand the aqueous geochemistry of rare earths and to predict their behavior in subsurface environments (Wood et al., 2002). Neodymium adsorption onto rutile (α-TiO_2) was investigated by potentiometric titration from 25 to 250°C, in NaCl media. This temperature range includes the extremes of natural environments, as well as field conditions associated with high-level radioactive waste storage. Rutile was selected for investigation owing to its insolubility over the wide temperature and pH range studied. Moreover, rutile is stable in the highly reducing conditions of the hydrogen-electrode concentration cell (HECC) utilized for the potentiometric titrations. Though rare in natural environments, rutile represents one extreme of metal-oxide surface chemistries, namely phases with high bulk dielectric constants (Sverjensky, 2001).

The potentiometric adsorption data for Nd^{3+} were modeled using the temperature compensated MUSIC model approach of Machesky et al. (2001), coupled with a Stern-based description of the EDL structure, and a tetradentate adsorption geometry. The tetradentate surface configuration was identified by Zhang et al. (2004) for Y^{3+} adsorption on the rutile (110) surface (the dominant crystal face developed on our powder materials (Ridley et al., 1999)), and we make the plausible assumption, based on the bare cation radii of these species, that the same geometry constitutes the primary mode of Nd^{3+} adsorption by our rutile powder as well. This assumption is further justified by more limited studies of Y^{3+} adsorption on the same rutile powders in NaCl media that demonstrate adsorption behavior very similar to Nd^{3+} at 25 and 50°C (Zhang et al., 2004).

2. EXPERIMENTAL

The rutile used in these experiments was the same as that used previously (Tioxide Specialties Ltd., Cleveland, UK), and it was subjected to similar pretreatment (Machesky et al., 1994, 1998; Ridley et al., 1999, 2002). The N_2-BET surface area of the cleansed rutile was 16.85 ($\pm$ 1) m^2/g, corresponding to an approximate particle size of 0.5 μm (Ridley et al., 1999).

The general method used to prepare the test, reference and titrant solutions has been described by Palmer and Drummond (1988), Palmer and Wesolowski (1993), and Ridley et al. (1998a,b, 1999, 2002). The $NdCl_3$ stock solution was prepared by dissolving 99.99% pure $NdCl_3 \cdot 6H_2O$, supplied by Johnson-Matthey, in deionized water, and subsequently acidifying the solution to 10^{-3}*m* HCl to limit hydrolysis (Wood et al., 2000). The exact Nd^{3+} content was quantified using a cation-exchange column (H^+ form, Dowex 50W-X8), and then titrating the eluate with a standardized NaOH stock solution. The compositions of the test, reference, and titrant solutions, prepared at 0.03 and 0.3*m* ionic strength, are given in Table 1.

The design and configuration of the hydrogen-electrode, concentration cell and auxiliary equipment used in this study, and the potentiometric titration procedure have been discussed in detail by Machesky et al. (1998) and Ridley et al. (1999, 2002). Briefly, potentiometric titrations were performed from 25 to 250°C. In each titration, ~1.5 g of rutile was suspended in 45 g of test solution, which was stirred magnetically throughout the experiment. The cell was allowed to equilibrate overnight (12–14 h) at temperature, with an initial cell configuration as follows:

$$\underset{\text{Test}}{\text{Pt, H}_2 \,|\, \text{HCl, NdCl}_3\text{, NaCl, TiO}_{2(cr)}} \;\|\; \underset{\text{Reference}}{\text{HCl, NaCl} \,|\, \text{H}_2\text{, Pt}}$$

Two independent sets of sorption data were obtained. In the first, "surface charge" data were obtained by equating the "excess" or "missing" protons in solution, in micromoles of H^+ per square meter of mineral surface, with the proton-induced surface charge via the relation, $\sigma_H = -F(\text{micromoles excess } H^+)/m^2$. The second set, referred to as "pH-edge" experiments (Dzombak and Morel, 1990), consisted of similar titrations during which samples were periodically withdrawn from the test solution through 0.2 μm filters into preweighed polypropylene syringes containing a known amount of high purity 1*m* HNO_3 for later analysis of the total dissolved Nd concentration by ICP-MS. Total dissolved Nd concentrations in samples withdrawn from the test solutions were always greater than those in method blanks which contained <0.5 μg/L total dissolved Nd.

In regressing the potentiometric data (Palmer and Drummond, 1988; Palmer and Wesolowski, 1993; Ridley et al., 1998a,b, 1999, 2002) no corrections for the effect of Nd-hydrolysis were included. The contribution of the $NdOH^{2+}$ species in all initial test solutions was minor (i.e., <2%) at all temperatures, as calculated using the first hydrolysis constants from Klungness and Byrne (2000) and Wood et al. (2002). In contrast, iterative calculations on our starting solutions (to estimate "real" ionic strengths) using the extended Debye-Hückel equation recommended by Helgeson and coworkers (e.g., Helgeson, 1969; Helgeson et al., 1981) and the $NaCl^o$ and Nd-chloride formation constants of Ho et al. (1994) and Migdisov and Williams-Jones (2002), respectively, indicate that Nd-chloride complexes predominate as temperature increases. For example, at 0.03*m* ionic strength $NdCl^{2+}$ and $NdCl_2^+$ comprised ~2.0 and 94% of the total Nd concentration at 25 and 250°C, respectively. Similarly, in 0.3*m* NaCl, $NdCl^{2+}$ and $NdCl_2^+$ comprised ~10 and 99% of the total Nd concentration at 25 and 250°C, respectively.

3. EXPERIMENTAL RESULTS

3.1. Net Surface Charge in NaCl Media with Neodymium Present

The net proton charge on the rutile surface in NaCl media was determined in earlier studies by the authors (Machesky et al., 1994, 1998; Ridley et al., 1999, 2002) (Fig. 1). In those studies, the point of zero net proton charge (pH_{znpc}) was defined as the pH value at which isothermal titration curves of 0.03, 0.3, and 1.0*m* NaCl intersected (Table 2).

The presence of Nd^{3+} enhanced dramatically the net negative proton charge development at the rutile surface (Fig. 1). The net proton charge data for solutions containing Nd^{3+} are listed in Appendix A. Similar behavior was documented by Ridley et al. (1999) for the adsorption of Ca^{2+} on rutile over the same temperature range. However, the

Table 1. Summary of the starting molal (mol/kg) solution compositions.

Reference		Test			Titrant	
$10^3\ m_{HCl}$	m_{NaCl}	$10^3\ m_{NdCl3}$	$10^3\ m_{HCl}$	m_{NaCl}	m_{NaOH}	m_{NaCl}
2.00	0.0280	0.997	1.00	0.0231	0.00999	0.0245
2.00	0.298	1.00	1.00	0.293	0.0100	0.320

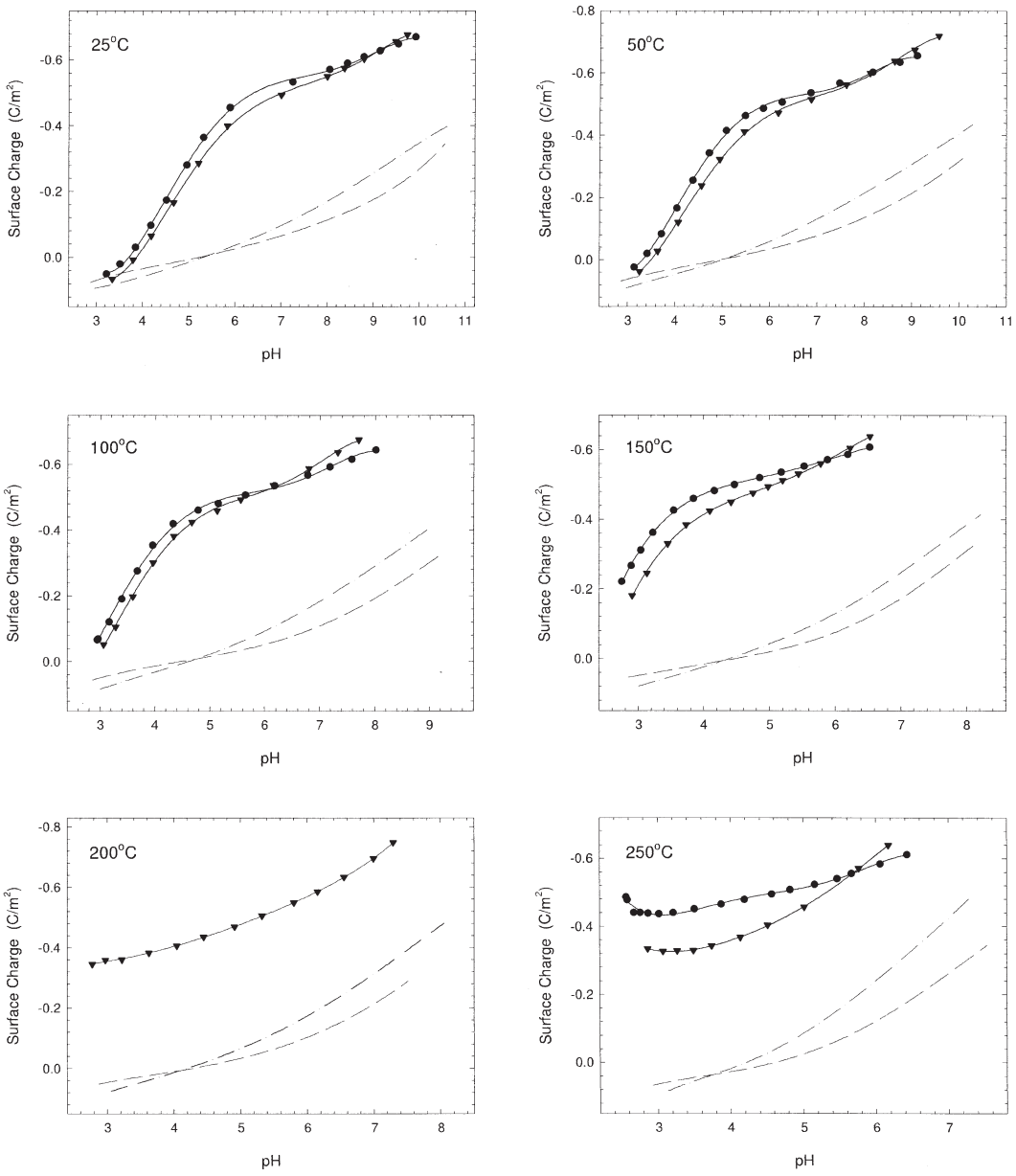

Fig. 1. The relationship between the proton charge and pH, for titrations performed in the absence (Machesky et al., 1998, 2001) and presence of Nd^{3+}, at each temperature studied. The dashed curves represent data in the absence of Nd^{3+} at I = 0.03*m* (broken line), and I = 0.3*m* (dash-dot line); and the symbols define Nd^{3+} (0.001*m* initial) adsorption at I = 0.03*m* (●), and I = 0.3*m* (▼). All curves represent fifth-order polynomial fits through the titration data.

magnitude of net negative proton charge enhancement is much greater for Nd^{3+} than for Ca^{2+}. As expected, the gain in negative proton charge development increases with cation charge in the order monovalent < divalent ≪ trivalent (i.e., $Na^{+} < Ca^{2+} \ll Nd^{3+}$). Furthermore, previous studies have reported similar behavior near room temperature for the adsorption of other di- and trivalent cations to metal oxide phases (Hohl and Stumm, 1976; Ardizzone et al., 1981; Jang and Fuerstenau, 1986; Gunnerison et al., 1994; Kosmulski, 1997a,b, 1999).

The present results (Fig. 1) clearly show that at all conditions the presence of Nd^{3+} results in a decrease in the apparent pH_{znpc} values. For example, the apparent pH_{znpc} value of rutile decreases by nearly 1.9 pH units at 25°C when 0.001*m* Nd^{3+} is present in solution; moreover, the negative shift in the apparent pH_{znpc} values increases at higher temperatures. By comparison, the study of Ridley et al. (1999) showed that Ca^{2+} sorbed to the rutile surface below the pH_{znpc} value only at temperatures above 200°C, whereas at lower temperatures Ca^{2+} adsorption commenced at pH values near the pH_{znpc}.

In Figure 2 the net proton charge curves in the presence of Nd^{3+} have been recast relative to the pH_{znpc} values in NaCl media (pH_{znpc} − pH), showing clearly the change in apparent pH_{znpc} values and the effect of temperature on Nd^{3+} adsorption

Table 2. Relevant MUSIC-Basic Stern model constants and variable parameter values.[a]

T (°C)	'A'	1/2 pK_w	log K_{H1}	log K_{H2}	pH_{znpc}	pH_{ppzc}	C_s (F/m^2)	SD_C	log K_M	SD_{KM}	log K_A	SD_{KA}	MSC
25	21.700	6.996	5.518	4.438	5.4	5.41	2.090	0.100	14.190	0.206	−2.700	1.178	4.52
50	20.490	6.635	5.210	4.191	5.1	5.12	2.096	0.115	14.280	0.216	−2.700	1.464	4.94
100	18.713	6.131	4.759	3.827	4.7	4.69	2.300	0.117	14.360	0.150	−2.192	0.509	4.99
150	17.647	5.820	4.488	3.609	4.4	4.44	2.662	0.164	14.513	0.136	−1.877	0.339	4.24
200	16.917	5.650	4.302	3.460	4.3	4.26	3.118	0.166	14.630	0.101	−1.465	0.154	4.63
250	16.452	5.598	4.184	3.365	4.2	4.15	5.081	0.507	14.868	0.018	−1.254	0.153	4.26

[a]'A' = a temperature-dependent constant; 1/2 pK_w = one-half the dissociation constant of water; log K_{Hn} = surface site protonation constants; pH_{znpc} = experimental value for the pH of zero net proton charge; pH_{ppzc} = pH value of the predicted pristine point of zero charge; C_S = capacitance value of the Stern Layer; SD_C = Standard Deviation of the Stern Layer capacitance value; log K_M and log K_A = cation and anion binding constants, respectively; SD_{KM} and SD_{KA} = Standard Deviation of the cation and anion binding constants (log units), respectively; and MSC = Model Selection Criteria. $K_{H1} : K_{H2} = 0.5 : 0.5$.

by rutile. At the start of the titrations (lowest pH) the net surface charge became progressively more negative with increasing temperature (Fig. 2); such that, only at 25 and 50°C was the rutile surface ever positively charged at any point in the titration. This increase in negative proton charge at initial titration conditions reflects the fraction of Nd^{3+} adsorbed, at pH values as low as 3. For example, by pH three 22% and greater than 90% of the total Nd^{3+} concentration was sorbed to the rutile surface at 100 and 250°C, respectively. The 200 and 250°C data were omitted from Figure 2 (and some later figures) because virtually all available Nd^{3+} was sorbed to the rutile surface at initial experimental conditions.

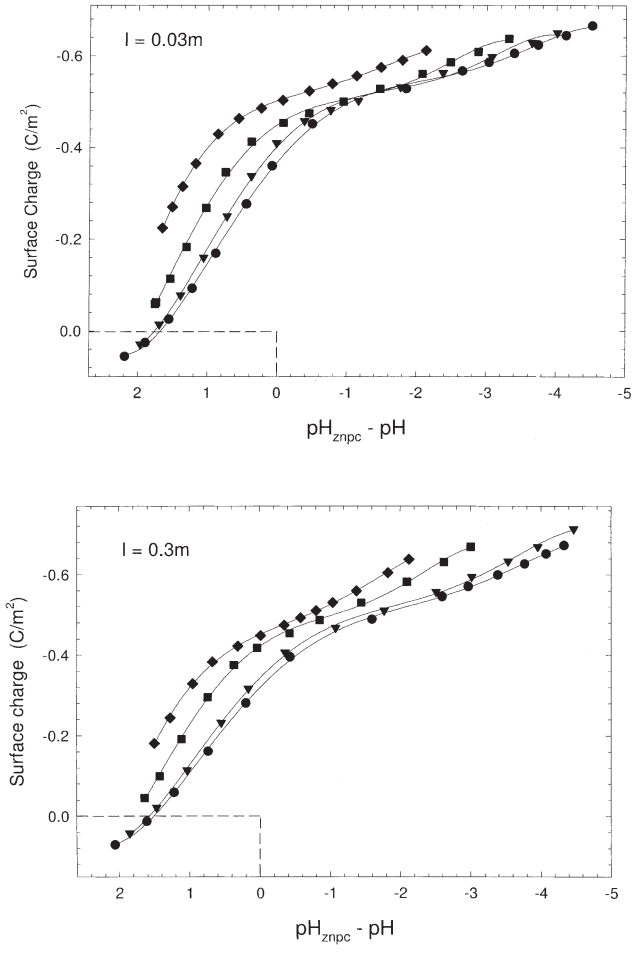

Fig. 2. The relationship between proton charge and (pH_{znpc} − pH) for Nd^{3+} adsorption. The symbols define experimental data at 25 (●), 50 (▼), 100 (■), and 150°C (◆); and the solid curves represent fifth-order polynomial fits through the titration data. The dashed vertical and horizontal lines represent the chosen pH_{znpc} values and the zero surface charge value, respectively.

In both Figures 1 and 2 a decrease in the slope of the net proton charge curves is evident above the pH_{znpc} values, resulting from the adsorption of virtually all available Nd^{3+}. The net proton charge curves begin to approximately parallel the curves observed in NaCl media alone, which is expected because Na^+ is then the only available counterion. To show more clearly how Nd^{3+} alone influences proton charge development, net proton charge curves (total proton charge minus proton charge in NaCl solutions only) as a function of (pH_{znpc} − pH) are presented in Figure 3. In effect, these curves approximate net proton release resulting from Nd^{3+} adsorption. The slopes of these curves decrease and approach zero at progressively more positive (pH_{znpc} − pH) values as temperature increases. Towards the end of the titrations, where (pH_{znpc} − pH) values are sufficiently negative (i.e., high pH values) the slopes of the net proton release curves generally become slightly negative. Our modeling results, presented below, rationalize these slightly negative net proton charge curves as resulting from a balance between chemical and electrostatic effects associated with the hydrolysis of adsorbed Nd^{3+} and the suppression of Na^+ adsorption by adsorbed Nd^{3+}, both of which are competing for the same tetradentate site. The effect of ionic strength on the sorption of Nd^{3+} to rutile is also evident from Figure 3. The net proton charge curves plateau at slightly higher values (C/m^2) for the 0.03*m* relative to 0.3*m* ionic strength data, because of the greater relative difference between the 0.03 and 0.3*m* proton charge curves in NaCl solutions only relative to those containing Nd^{3+} (Fig. 1).

3.2. Adsorption "pH Edge" Results

In Figure 4 the adsorption "pH edge" data are presented in terms of (pH_{znpc} − pH), rather than pH, thus normalizing for the observed decrease in the pH_{znpc} values with increasing temperature. Normalizing the data in this manner enables the influence of temperature to be resolved more clearly (Kosmul-

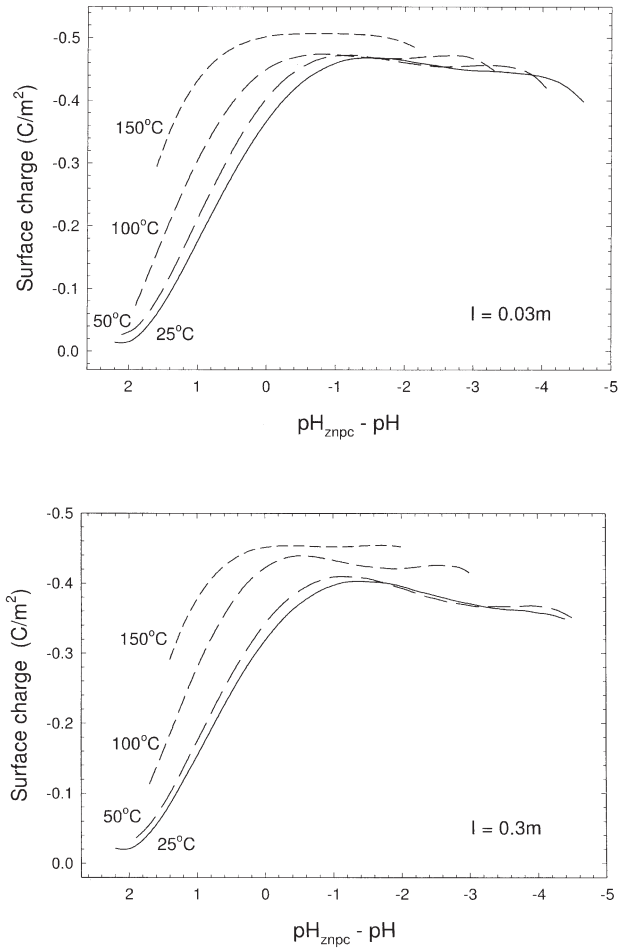

Fig. 3. Net proton charge curves as a function of (pH_{znpc} − pH). Briefly the net surface charge term was obtained by subtracting the surface charge curve in NaCl media from the corresponding surface charge curve in the presence of Nd^{3+} (Fig. 1).

ski, 1996): adsorption "pH edges" shift to lower (pH_{znpc} − pH) values with increasing temperature. Moreover, at 200 and 250°C virtually all available Nd^{3+} was adsorbed at the start of the titrations. The Nd^{3+} adsorption data are provided in Appendix B. A slight ionic strength effect is also apparent from Figure 4, as the adsorption "pH edge" is at slightly higher (pH_{znpc} − pH) values at 0.3*m* relative to 0.03*m* ionic strength. Similarly, the effect of ionic strength on Nd^{3+} adsorption is also evident from the proton charge data (Fig. 1), where the net negative proton charge in 0.03*m* is enhanced slightly relative to the 0.3*m* ionic strength data. These ionic strength effects probably result from increased competition from Na^+. The ionic strength dependence of cation uptake by metal oxide surfaces is often taken to indicate "outer sphere" vs. "inner sphere" adsorption (Hayes and Katz, 1996). The slight ionic strength effect observed for Nd^{3+} is consistent with "inner sphere" adsorption to rutile. By comparison, significant ionic strength dependence was observed for the adsorption of Ca^{2+} on the same rutile powder (Ridley et al., 1999, 2004), suggesting, as anticipated, that Nd^{3+} ions are adsorbed more strongly by the rutile surface. However, this is not a result of "outer sphere" sorption of Ca^{2+} but only less effective competition of this weakly bound divalent cation with the more abundant background electrolyte cation, Na^+, in the tetradentate binding site, as has been demonstrated by X-ray standing wave studies for Rb^+ and Sr^{2+} and MD simulations for Na^+, Rb^+, Ca^{2+} and Sr^{2+} (Zhang et al., 2004).

The data presented in Figures 3 and 4 can be used to estimate proton stoichiometric ratios (moles H^+ released / moles Nd^{3+} adsorbed) for our experimental conditions. Briefly, the H^+-released term comes directly from Figure 3, and the corresponding moles Nd^{3+}-adsorbed term comes from the adsorption "pH edge" data (Fig. 4). Observed proton stoichiometric ratios can result from charge redistribution processes in the electrical double layer region, as well as chemical effects such as proton release from specific surface hydroxyl groups, or surface induced hydrolysis (Fokkink et al., 1987; Dzombak and Morel, 1990).

Proton stoichiometric ratios were calculated only for the portion of a titration curve having less than 100% of the total Nd^{3+} adsorbed. In addition, at some high-temperature experimental conditions the "pH edge" data were limited, in which case the proton stoichiometetric ratio was calculated from the initial "pH edge" value (i.e., the first point of the titration). For this study, proton stoichiometric ratios ranged between 2.3 and 2.8 in 0.03*m* ionic strength and between 2.3 and 2.6 in 0.3*m* ionic strength with the highest values usually corresponding to higher surface coverages. This slight decrease in proton stoichiometric ratios with increasing ionic strength was also observed by Ridley et al. (1999) for Ca^{2+} adsorption by rutile. In that study, the average ratio decreased from 1.5 to 1.3 at 0.03 and 0.3*m* NaCl, respectively. Similarly, Fokkink et al. (1990) found a small decrease in the proton stoichiometric ratios with increasing ionic strength (0.02 to 0.20 M KNO_3) for Cd^{2+} adsorption by rutile and hematite between 20 and 60°C. The proton stoichiometric ratios derived in the present study are higher than Kosmulski (1997a) reported for the adsorption of

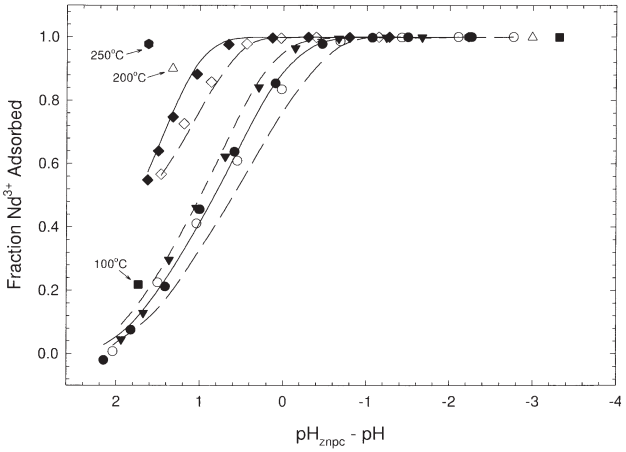

Fig. 4. Adsorption "pH edge" data as a function of (pH_{znpc} − pH), where the symbols represent experimental temperatures of 25 (●), 50 (▼), and 150°C (◆). The closed and open symbols represent 0.03 and 0.3*m* ionic strength data, respectively. MUSIC Model best-fit curves for a tetradentate surface complex, hydrolysis of the tetradentate surface complex and a three-layer description of the EDL structure are represented by the curves. The curves at 25 and 150°C represent fits at 0.03 (solid line) and 0.3*m* (broken line), and 50°C (dashed line). All model parameter values are defined in the text and are given in Tables 2 and 3.

comparable trivalent cations on alumina (ratios of 1.9 and 1.8 were reported for Y^{3+} and Gd^{3+}, respectively). Furthermore, no distinct temperature trends were apparent, as also observed for Ca^{2+} by Ridley et al. (1999) suggesting that the actual chemical and/or electrostatic factors governing Nd^{3+} adsorption do not change significantly with increasing temperature.

4. SURFACE COMPLEXATION MODELING

All modeling efforts followed our previous work utilizing the temperature-compensated MUSIC model (Machesky et al., 2001; Ridley et al., 2002, 2004). Briefly, the MUSIC model specifically considers the crystal structure of minerals, including types, concentrations, and bonding geometries of the ≡*S*-OH surface sites present on metal-(hydr)oxide phases. Given this information, the MUSIC model predicts the proton binding constants for a variety of terminal oxygen sites from an independent empirical model based on the Pauling bond-valence principle (Hiemstra et al., 1989, 1996).

For rutile, Jones and Hockey (1971) have suggested that the predominant crystallographic planes of many powdered rutile samples are the (110), (100), and (101) faces, in a ratio of ~0.6:0.2:0.2. This is approximately true for our powdered rutile since the (110) surface clearly predominates (Ridley et al., 2002). From this representation of the rutile surface, two independent surface groups predominate: singly coordinated (or terminal) hydroxyls and doubly coordinated (or bridging) surface oxygen atoms (Fig. 5), in an ideal 1:1 ratio. These surface sites and their protonation reactions are represented by:

$$\equiv \mathrm{TiOH}^{-0.254} + \mathrm{H}^{+} = \equiv \mathrm{TiOH}_2^{+0.746} \quad \mathrm{K_{H1}} \qquad (1)$$

$$\equiv \mathrm{Ti_2O}^{-0.405} + \mathrm{H}^{+} = \equiv \mathrm{Ti_2OH}^{+0.595} \quad \mathrm{K_{H2}} \qquad (2)$$

The protonation constants for these reactions, the corresponding pH values at the pristine point of zero charge (pH_{ppzc}) and the experimental pH_{znpc} values, are discussed in greater detail by Machesky et al. (2001). The data presented in Machesky et al. (2001) and Ridley et al. (2002) were refit using the MUSIC model assuming that the Ti-O bond lengths of the Ti-OH and Ti_2-O surface groups were 1.916 and 1.890 Å, respectively. These bond lengths were adjusted slightly (<0.1 Å) from those determined from ab initio calculations (Bandura and Kubicki, 2003) to closely match the experimental pH_{znpc} at 25°C of 5.4. This resulted in small changes in the surface site charges and K_H values in equations (1–2), relative to the values used in our previous studies. In all modeling efforts, a total surface site concentration of 12.5 sites/nm^2 (20.8 μmol/m^2) was assumed (Table 2), as dictated by crystallographic constraints. Previously, both Na^+ and Cl^- counterions were assumed to bind in monodentate fashion (e.g., Machesky et al., 2001; Ridley et al., 2004). However, the NaCl-only proton charge data were refit here (Fig. 5), assuming that the actual Na^+ adsorption configuration is tetradentate, as supported by MD simulations of Na^+ interactions with the rutile (110) surface, and by analogous X-ray standing wave results for Rb^+ adsorption on rutile (Zhang et al., 2004). The MUSIC model representation of this reaction is,

$$2(\equiv \mathrm{TiOH}^{-0.254}) + 2(\equiv \mathrm{Ti_2O}^{-0.405}) + \mathrm{Na}^{+} = [(\equiv \mathrm{TiOH}^{-0.254})_2(\equiv \mathrm{Ti_2O}^{-0.405})_2] - \mathrm{Na}^{+} \quad \mathrm{K_M} \qquad (3)$$

The other model fitting parameters were the Cl^- binding constant, K_A, assumed to be monodentate and equal for binding to either the terminal or bridging site, and a Stern layer capacitance value, C_s. The choice of monodentate chloride binding was arbitrary, since no clear evidence of specific chloride binding at rutile surfaces is indicated by X-ray or MD simulation (Zhang et al., 2004). However, since chloride binding to the surface is weak, this is not a critical model parameter. All parameters from the MUSIC model and NaCl-only data fits are summarized in Table 2; these values were held constant when modeling the Nd^{3+} adsorption data. Tables 2 and 3 include standard deviations (or confidence intervals) for the best-fit parameter values (SD) and model selection criterion (MSC) values. The SD values were estimated separately for each parameter (i.e., no correlation between the fitted parameters); moreover, it was assumed that the parameters behaved linearly near the best-fit solution. The MSC value is a normalized inverse form of the Akaike Information Criterion (Akaike, 1976). It is a measure of the goodness of fit of the model, with larger values signifying better fits.

When modeling the Nd^{3+} data, all net proton charge and adsorption "pH edge" data at each temperature studied were fit simultaneously except for 250°C where only the 0.03*m* net proton charge data were fit since the corresponding 0.30*m* data appear anomalous (see below). As with the NaCl data, we made the plausible assumption that the tetradentate, inner sphere, adsorption geometry found by Zhang et al. (2004) for Y^{3+} adsorption on the rutile (110) surface constitutes the primary mode of Nd^{3+} adsorption by our rutile powder as well (Fig. 5). This assumption is justified by more limited studies of Y^{3+} adsorption on the same rutile powders in NaCl media (Zhang et al., 2004) that demonstrate the very similar adsorption behavior of Nd^{3+} and Y^{3+}. Additionally, the X-ray and MD simulation results of Zhang et al. (2004) indicate that all mono-, di- and trivalent cations with bare ionic radii greater than or equal to that of Y^{3+} bind specifically at the tetradentate site on rutile (110). The representation of this reaction is comparable to the Na^+ adsorption reaction.

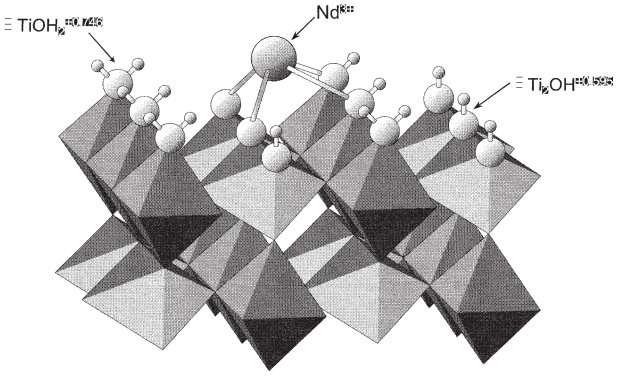

Fig. 5. Negatively charged rutile (110) surface with Nd^{3+} binding in a tetradentate configuration, involving two terminal (≡$TiOH^{-0.254}$) and two bridging (≡$Ti_2O^{-0.405}$) surface groups. Note that there is a 3-coordinated oxygen atom in the surface Ti-O plane immediately beneath the sorbed cation. This surface oxygen may or may not participate in the binding of the sorbed cation, but the MUSIC model indicates that it does not protonate in the 0–14 pH range.

Table 3. MUSIC-Basic Stern model constants and variable parameter values for the adsorption of Nd^{3+} onto rutile in a tetradentate configuration.[a]

T (°C)	pH_{znpc}	C_1 (F/m^2)	SD_C	log K TET-Nd	SD logK TET-Nd	log K TET-NdOH	SD log K TET-NdOH	log K TET-$Nd(OH)_2$	SD logK TET-$Nd(OH)_2$	log K TET-$Nd(OH)_3$	SD logK TET-$Nd(OH)_3$	MSC^a	MSC^b
25	5.4	6.6	0.91	23.1	0.20	15.0	0.46	7.9	0.27			5.30	4.99
50	5.1	6.4	0.77	23.4	0.17	15.6	0.29	9.1	0.22			5.62	4.55
100	4.7	5.0	1.89	24.7	0.57	16.6	5.20	13.0	0.33			3.84	2.72
150	4.4	5.5	2.00	26.0	0.64	17.6	5.01	14.9	0.22	10.1	0.27	5.71	4.35
200	4.3	5.5		26.5		18.2		17.6	0.45	10.6	1.30	2.65	0.92
250	4.2	5.5		27.2		18.9		19.5	0.22	13.8	0.26	2.17	−0.79

[a]pH_{znpc} = experimental value for the pH of zero net proton charge; C_1 = capacitance value for the Nd-binding plane; log $K_{TET\text{-}Nd}$ = Nd^{3+} binding constant in a tetradentate configuration; log $K_{TET\text{-}Nd(OH)n}$ = binding constants for the hydrolysis of surface adsorbed Nd^{3+}; SD_n = Standard Deviation of the relevant parameter with a blank cell signifying a parameter value that was held constant during fitting; MSC^a = Model Selection Criteria when the variable fitting parameters included C_1, log $K_{TET\text{-}Nd}$, and log $K_{TET\text{-}Nd(OH)n}$; and MSC^b = Model Selection Criteria when only C_1 and log $K_{TET\text{-}Nd}$ were the variable fitting parameters.

$$2(\equiv TiOH^{-0.254}) + 2(\equiv Ti_2O^{-0.405}) + Nd^{3+} = [(\equiv TiOH^{-0.254})_2(\equiv Ti_2O^{-0.405})_2] - Nd^{3+} \quad (4)$$

The EDL structure was expanded from the basic Stern to a three-layer model, with the Nd-binding plane positioned closest to the rutile surface. A sketch of the EDL structure is given in Figure 6, and from the surface outward comprises, protonation at the mineral surface (defined by K_{H1} and K_{H2}), adsorption of Nd^{3+} (K_{Nd}), binding of the background electrolyte ions at the outer Stern layer (K_M and K_A), and the diffuse layer. The assumption that chloride binding occurs at the same plane as that of Na^+ is not consistent with the MD simulation results, which indicate that chloride ions never approach the surface as closely as do cations, but since the chloride interaction is so weak, this does not significantly affect the model results for Nd^{3+} binding. In the absence of the X-ray data of Zhang et al. (2004) used to constrain our modeling efforts, various other inner-sphere surface complexes of Nd^{3+} would have been equally reasonable. Some examples include, [≡$TiOH^{-0.254}$]-Nd^{3+}, [≡$Ti_2O^{-0.405}$]-Nd^{3+}, [(≡$TiOH^{-0.254}$)$_2$]-Nd^{3+}, [(≡$Ti_2O^{-0.405}$)$_2$]-Nd^{3+}, and [(≡$TiOH^{-0.254}$)(≡$Ti_2O^{-0.405}$)]-Nd^{3+}.

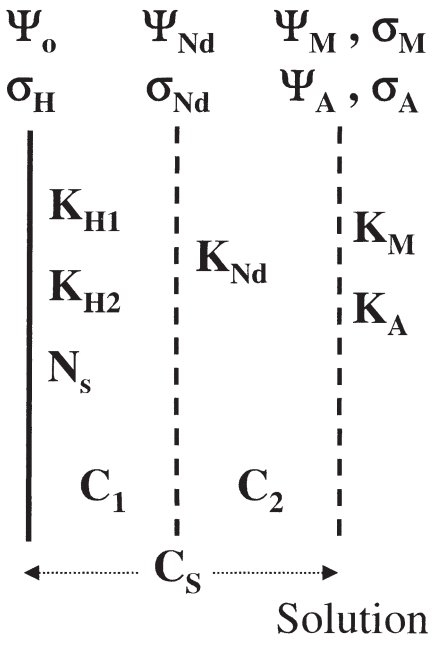

Fig. 6. Schematic representation of a three-layer description of the EDL structure combined with the MUSIC model. The notation represents protonation (K_{Hn}), cation (K_M), anion (K_A) and neodymium (K_{Nd}) binding constants; Ψ_n and σ_n are the potential and charge at the binding planes, respectively; C_S is the capacitance value of the Stern Layer; and N_S is the surface site concentration, fixed at 20.8 μmol/m^2 (12.5 sites/nm^2).

Permitting hydrolysis of the adsorbed Nd^{3+} markedly improved the fit to the net proton charge curves particularly at temperatures ≥100°C and at high pH (Fig. 7). These hydrolysis reactions are represented as,

$$[(\equiv TiOH^{-0.254})_2(\equiv Ti_2O^{-0.405})_2] + Nd^{3+} + H_2O = [(\equiv TiOH^{-0.254})_2(\equiv Ti_2O^{-0.405})_2] - NdOH^{2+} + H^+ \quad (5)$$

$$[(\equiv TiOH^{-0.254})_2(\equiv Ti_2O^{-0.405})_2] + Nd^{3+} + 2H_2O = [(\equiv TiOH^{-0.254})_2(\equiv Ti_2O^{-0.405})_2] - Nd(OH)_2^+ + 2H^+ \quad (6)$$

$$[(\equiv TiOH^{-0.254})_2(\equiv Ti_2O^{-0.405})_2] + Nd^{3+} + 3H_2O = [(\equiv TiOH^{-0.254})_2(\equiv Ti_2O^{-0.405})_2] - Nd(OH)_3^o + 3H^+ \quad (7)$$

It was assumed that both unhydrolyzed and hydrolyzed Nd ions were tetrahedrally coordinated at the same binding plane.

The variable fitting parameters are, therefore, four potential Nd^{3+} binding constants (for Eqns. 4 to 7), and the capacitance value (F/m^2) for the Nd-binding plane, C_1. The Stern layer capacitance values are related by,

$$1/C_S = 1/C_1 + 1/C_2 \quad (8)$$

where C_S = the Stern layer capacitance as determined from fitting the NaCl-only data (Table 2), and C_2 = the capacitance value of the outer counterion binding plane, determined by difference. In all modeling efforts, the activity coefficient for Nd^{3+} was estimated using the square of charge approximation (Meissner and Kusik, 1972), such that $\gamma_{Nd3+} = (\gamma_{\pm NaCl})^9$. Mean molal stoichiometric activity co-

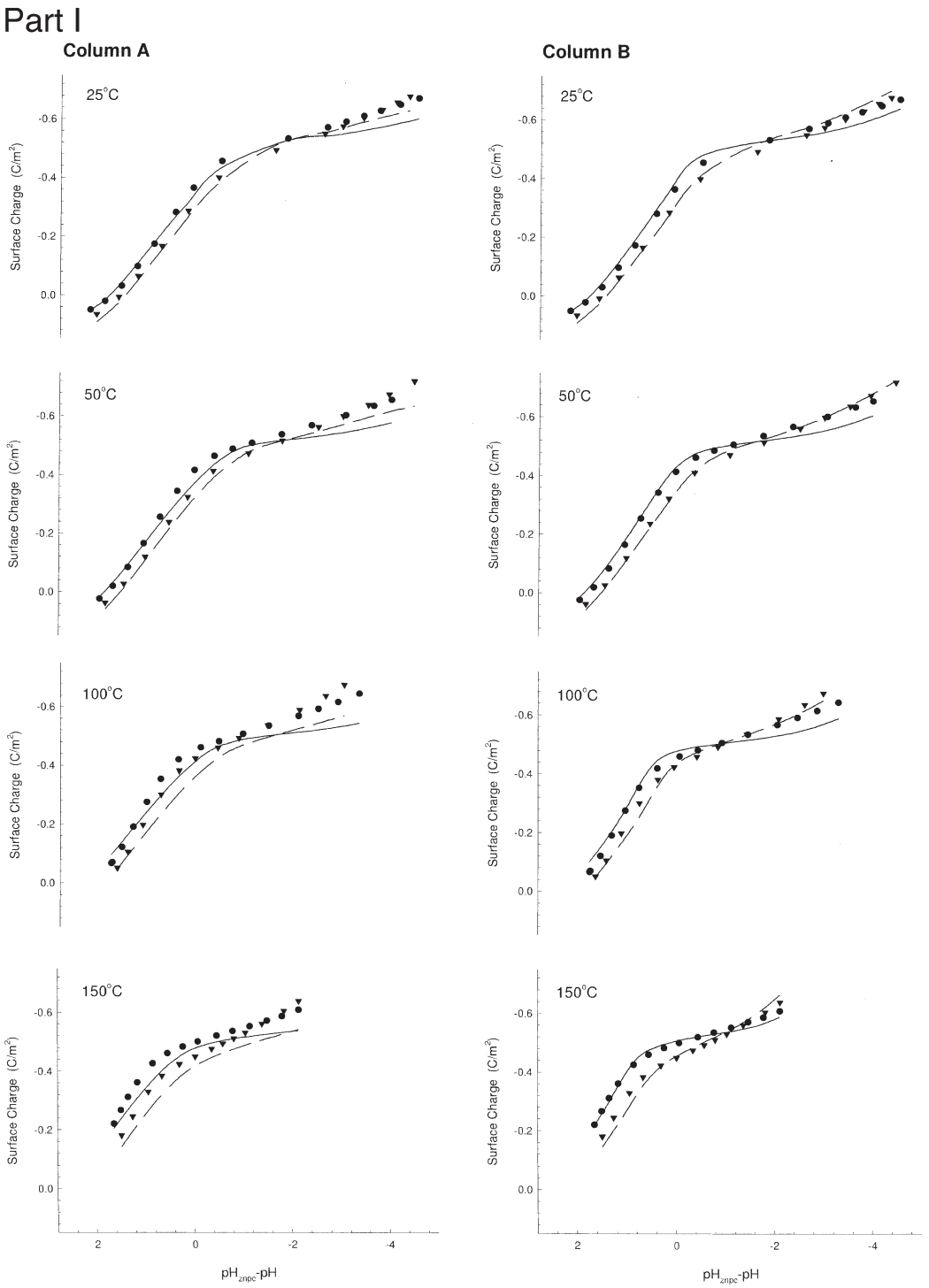

Fig. 7. MUSIC Model fits of proton charge and (pH_{znpc} − pH), with the experimental data shown as symbols at 0.03*m* (●) and 0.3*m* (▼), and the best-fit curves shown as solid (0.03*m*) and dashed (0.3*m*) lines. In the left-hand column (column A) the variable fitting parameters included a single tetradentate surface complex (log $K_{TET\text{-}Nd}$) and binding plane (C_1) capacitance value; whereas the right-hand column (column B) provides fits that also include binding constants for the hydrolysis of the Nd-surface species (log $K_{TET\text{-}Nd(OH)n}$).

efficients for NaCl were taken from Pitzer et al. (1984), and it was assumed that $\gamma_{Na+} = \gamma_{Cl-} = \gamma_{\pm NaCl}$. This approach implicitly accounts for at least some Nd-chloride complexing, and by way of comparison the free Nd^{3+} activities of our starting solutions were also estimated by iterative calculations of the "real" ionic strength (Helgeson, 1969) considering Nd^{3+}, $NdCl^{2+}$, $NdCl_2^{+}$, Na^{+}, Cl^{-}, and $NaCl^{o}$ as solution species, in conjunction with $NaCl^{o}$ and Nd-chloride

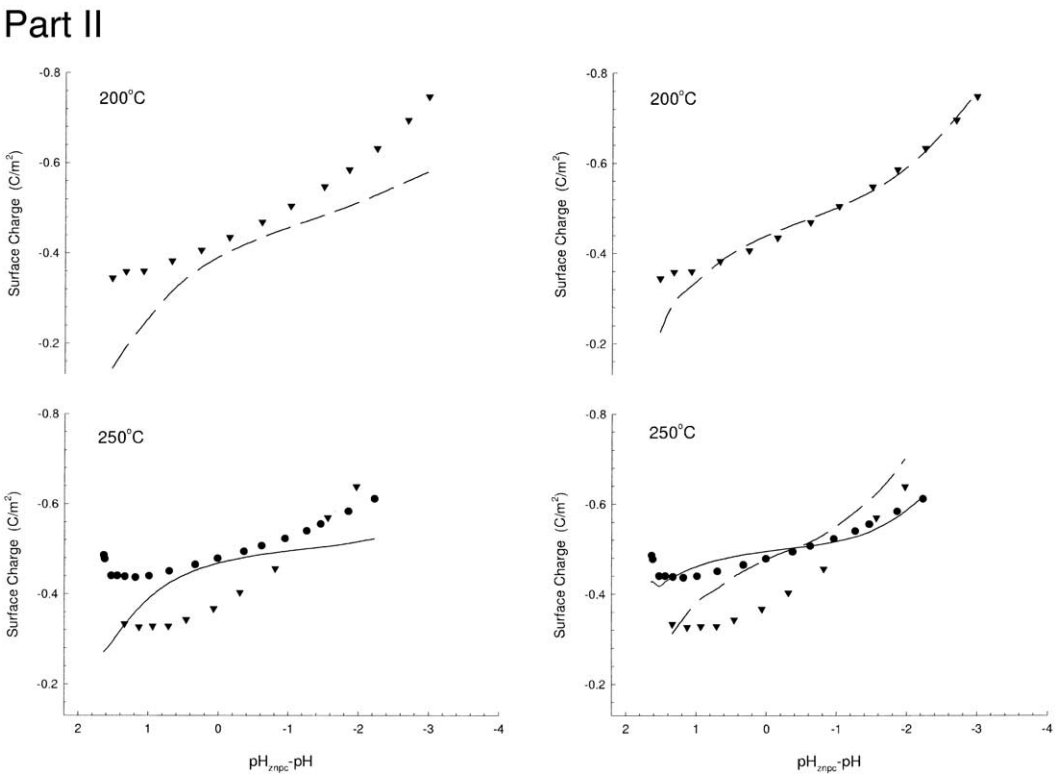

Fig. 7. (continued)

formation constants from Ho et al. (1994) and Migdisov and Williams-Jones (2002), respectively. Between 25 and 150°C free Nd^{3+} activities estimated from the square of charge approximation were ~0.80 and 0.40 of those from the "real" ionic strength-solution speciation approach at 0.03 and 0.30*m*, respectively. These ratios increased to 1.4 and 1.1 at 200°C, and 8.4 and 4.5 at 250°C. Given the approximations and uncertainties inherent in either approach, the level of agreement is actually quite reasonable (within a factor of 10). Modeling efforts confirmed that arbitrarily higher and lower Nd^{3+} activities had the expected effect of proportionately lowering and raising $K_{TET\text{-}Nd}$ (Eqn. 10, below), respectively. In any case, the comparison provides perspective for the square of charge approach used to estimate Nd^{3+} activity in this study.

The model parameter values for tetradentate adsorption of Nd^{3+} onto rutile were formulated as follows. The total surface site concentration is given by

$$\begin{aligned} N_S = {} & [TiOH^{z_1}] + [TiOH_2^{(z_1+z_H)}] + [TiOH_2^{(z_1+z_H)} - Cl^-] \\ & + [Ti_2O^{z_2}] + [Ti_2OH^{(z_2+z_H)}] + [Ti_2OH^{(z_2+z_H)} - Cl^-] \\ & + \left[(TiOH^{z_1})_2(Ti_2O^{z_2})_2 - Na^+\right] + \left[(TiOH^{z_1})_2(Ti_2O^{z_2})_2 - Nd^{3+}\right] \\ & + \left[(TiOH^{z_1})_2(Ti_2O^{z_2})_2 - NdOH^{2+}\right] \\ & + \left[(TiOH^{z_1})_2(Ti_2O^{z_2})_2 - Nd(OH)_2^+\right] \\ & + \left[(TiOH^{z_1})_2(Ti_2O^{z_2})_2 - Nd(OH)_3^0\right] \end{aligned} \quad (9)$$

where $z_1 = -0.254$ and $z_2 = -0.405$ are the charges for the terminal and bridged surface groups, respectively, and z_H = hydrogen ion charge (+1). All parameters for the surface protonation constants and electrolyte ion binding constants are given in Table 2. The tetradentate binding constant for reaction 4 was a fitting parameter and is defined as,

$$\begin{aligned} K_{TET-Nd} = {} & \left[(\equiv TiOH^{-0.254})_2(Ti_2O^{-0.405})_2 - Nd^{3+}\right] / \\ & \left\{\left[\equiv TiOH^{-0.254}\right]^2\left[\equiv Ti_2O^{-0.405}\right]^2\left[Nd^{3+}\right]_b \right. \\ & \left. (\gamma_{Nd3+}) \exp(-z_{Nd}F\Psi_{Nd}/RT)\right\} \end{aligned} \quad (10)$$

where $[Nd^{3+}]_b$ = free neodymium concentration (molal) in the bulk solution, γ_{Nd3+} = molal stoichiometric activity coefficient of Nd^{3+} at a given ionic strength and temperature, as defined above, z_{Nd} = neodymium charge (+3), and Ψ_{Nd} = potential at the Nd binding plane. Similarly, the surface hydrolysis constants are defined as,

$$\begin{aligned} K_{TET-NdOH} = {} & \left[(\equiv TiOH^{-0.254})_2(\equiv Ti_2O^{-0405})_2 \right. \\ & \left. - NdOH^{2+}\right](H^+)_b \exp(-z_HF\Psi_M/RT) / \\ & \left\{a_w\left[\equiv TiOH^{-0.254}\right]^2\left[\equiv Ti_2O^{-0.405}\right]^2\left[Nd^{3+}\right]_b \right. \\ & \left. (\gamma_{Nd3+}) \exp(-z_{Nd}F\Psi_{Nd}/RT)\right\} \end{aligned} \quad (11)$$

$$\begin{aligned} K_{TET-Nd(OH)2} = {} & \left[(\equiv TiOH^{-0.254})_2(\equiv Ti_2O^{-0405})_2 \right. \\ & \left. - Nd(OH)_2^+\right](H^+)_b^2 \exp(-z_HF\Psi_M/RT) / \\ & \left\{a_w^2\left[\equiv TiOH^{-0.254}\right]^2\left[\equiv Ti_2O^{-0.405}\right]^2\left[Nd^{3+}\right]_b \right. \\ & \left. (\gamma_{Nd3+}) \exp(-z_{Nd}F\Psi_{Nd}/RT)\right\} \end{aligned} \quad (12)$$

$$K_{TET-Nd(OH)3} = \left[(\equiv TiOH^{-0.254})_2(\equiv Ti_2O^{-0405})_2 - Nd(OH)_3^0\right](H^+)_b^3 \exp(-z_H F\Psi_M/RT)/\left\{a_w^3\left[\equiv TiOH^{-0.254}\right]^2\left[\equiv Ti_2O^{-0.405}\right]^2\left[Nd^{3+}\right]_b (\gamma_{Nd3+}) \exp(-z_{Nd}F\Psi_{Nd}/RT)\right\} \quad (13)$$

where $(H^+)_b$ = bulk hydrogen ion activity, Ψ_M = the potential at the outer Stern plane, a_w = activity of water and all other parameters are defined above. These formulations of the tetradentate binding constants are based on the concentration of surface species (mol/m^2), assuming unit activity coefficients for surface species. The capacitance value (F/m^2) of the Nd binding plane (C_1) was an additional fitting parameter, used to determine the associated surface, inner binding plane and Stern layer potentials. These potentials can be expressed as,

$$\Psi_0 = (\sigma_H/C_1) + \Psi_{Nd} \quad (14)$$

$$\Psi_{Nd} = (\sigma_{Nd} + \Psi_0 C_1 + \Psi_M C_2)/(C_1 + C_2) \quad (15)$$

$$\Psi_d = \Psi_M = \Psi_A = (2RT/F)\ \text{arcsinh}\ (-\sigma_d/(8RT\varepsilon_0\varepsilon_b\, I\, \rho_s)^{1/2}) \quad (16)$$

where ε_0 = permittivity of vacuum = 8.854×10^{-12}, ε_b = bulk dielectric constant of water at a given temperature (Archer and Wang, 1990) and ionic strength (Helgeson et al., 1981), I = stoichiometric molal ionic strength, and ρ_s = solution density which was taken from tabulated properties of NaCl solutions (Pitzer et al., 1984). The solution density term is necessary since the Gouy-Chapman theory, which is used to calculate Ψ_d above, is typically formulated in terms of molar (per unit volume) concentration units.

The charge associated with each layer is defined as,

σ_{PS} = proton surface charge,

$$\sigma_{PS} = F\Big\{\left[TiOH_2^{(zl+zH)}\right](z_1 + z_H) + \left[TiOH_2^{(zl+zH)} - Cl^-\right](z_1 + z_H) + \left[TiOH^{zl}\right](z_1) + \left[Ti_2OH^{(z2+zH)}\right](z_2 + z_H) + \left[Ti_2OH^{(z2+zH)} - Cl^-\right](z_2 + z_H) + \left[Ti_2O^{z2}\right](z_2) + \left[(TiOH^{zl})_2(Ti_2O^{z2})_2 - Na^+\right](2(z_1 + z_2)) + \left[(TiOH^{zl})_2(Ti_2O^{z2})_2 - Nd^{3+}\right](2(z_1 + z_2)) + \left[(TiOH^{zl})_2(Ti_2O^{z2})_2 - NdOH^{2+}\right](2(z_1 + z_2)) + \left[(TiOH^{zl})_2(Ti_2O^{z2})_2 - Nd(OH)_2^+\right](2(z_1 + z_2)) + \left[(TiOH^{zl})_2(Ti_2O^{z2})_2 - Nd(OH)_3^0\right](2(z_1 + z_2))\Big\} \quad (17)$$

σ_{Nd} = charge at the Nd^{3+} binding plane (inner Stern layer),

$$\sigma_{Nd} = F\left\{\left[(TiOH^{z_1})_2(Ti_2O^{z_2})_2 - Nd^{3+}\right](z_{Nd})\right\} \quad (18)$$

σ_M = outer Stern layer cation charge (due to hydrolyzed Nd^{3+} species and Na^+),

$$\sigma_M = F\Big\{\left[(TiOH^{z_1})_2(Ti_2O^{z_2})_2 - NdOH^{2+}\right](z_{Nd} + z_{OH}) + \left[(TiOH^{z_1})_2(Ti_2O^{z_2})_2 - Nd(OH)_2^+\right](z_{Nd} + 2z_{OH}) + \left[(TiOH^{z_1})_2(Ti_2O^{z_2})_2 - Nd(OH)_3^0\right](z_{Nd} + 3z_{OH}) + \left[(TiOH^{z_1})_2(Ti_2O^{z_2})_2 - Na^+\right](z_M)\Big\} \quad (19)$$

σ_A = outer Stern layer anion charge (due to Cl^-),

$$\sigma_A = F\left\{\left[(TiOH_2^{(z_1+z_H)} - Cl^-] + [Ti_2OH^{(z_2+z_H)} - Cl^-]\right)(z_A)\right\} \quad (20)$$

where z_M and z_A = sodium (+1) and chloride (−1) charge, respectively, and z_{OH} = hydroxyl ion charge (−1).

σ_S = Total Stern layer charge,

$$\sigma_S = \sigma_M + \sigma_A + \sigma_{Nd} \quad (21)$$

σ_d = uncompensated or diffuse layer charge,

$$\sigma_d = -F\Big\{\left[TiOH^{z_1}\right](z_1) + \left[TiOH_2^{(z_1+z_H)}\right](z_1 + z_H) + \left[TiOH_2^{(z_1+z_H)} - Cl^-\right](z_1 + z_H + z_A) + \left[Ti_2O^{z_2}\right](z_2) + \left[Ti_2OH^{(z_2+z_H)}\right](z_2 + z_H) + \left[Ti_2OH^{(z_2+z_H)} - Cl^-\right](z_2 + z_H + z_A) + \left[(TiOH^{z_1})_2(Ti_2O^{z_2})_2 - Na^+\right](2(z_1 + z_2) + z_M) + \left[(TiOH^{z_1})_2(Ti_2O^{z_2})_2 - Nd^{3+}\right](2(z_1 + z_2) + z_{Nd}) + \left[(TiOH^{z_1})_2(Ti_2O^{z_2})_2 - NdOH^{2+}\right](2(z_1 + z_2) + z_{Nd} + z_{OH}) + \left[(TiOH^{z_1})_2(Ti_2O^{z_2})_2 - Nd(OH)_2^+\right](2(z_1 + z_2) + z_{Nd} + 2z_{OH}) + \left[(TiOH^{z_1})_2(Ti_2O^{z_2})_2 - Nd(OH)_3^0\right](2(z_1 + z_2) + z_{Nd} + 3z_{OH})\Big\} \quad (22)$$

Electroneutrality requires that,

$$\sigma_{PS} + \sigma_{Nd} + \sigma_M + \sigma_A + \sigma_d = 0 \quad (23)$$

Hydrolysis of adsorbed Nd^{3+} contributes to the measured net proton charge as follows,

$$\sigma_{Hydrol} = -F\Big\{\left[(TiOH^{zl})_2(Ti_2O^{z2})_2 - NdOH^{2+}\right](z_H) + \left[(TiOH^{zl})_2(Ti_2O^{z2})_2 - Nd(OH)_2^+\right](2z_H) + \left[(TiOH^{zl})_2(Ti_2O^{z2})_2 - Nd(OH)_3^0\right](3z_H)\Big\} \quad (24)$$

Finally, the net proton charge is,

$$\sigma_H = \sigma_{PS} + \sigma_{Hydrol} \quad (25)$$

Modeling was conducted using combined least-squares and trial-and-error fitting approaches. The two approaches were necessary because of the large number of potentially variable parameters (C_1, and four possible Nd binding constants). Typically, first-cut solutions to the model parameters were obtained by trial-and-error while monitoring model statistical output (MSC values, parameter standard deviations and correlations). Then, in an attempt to improve the goodness of fit, true least-squares fitting was performed with combinations of 1–3 model parameters. It was not possible to freely vary more than three parameters simultaneously and converge to a solution. Additional iterations of trial-and-error and least-squares fits were performed as necessary to obtain the final set of variable parameter values, corresponding best-fit σ_H and adsorption "pH edge" values, MSC values, and parameter standard deviations and correlations.

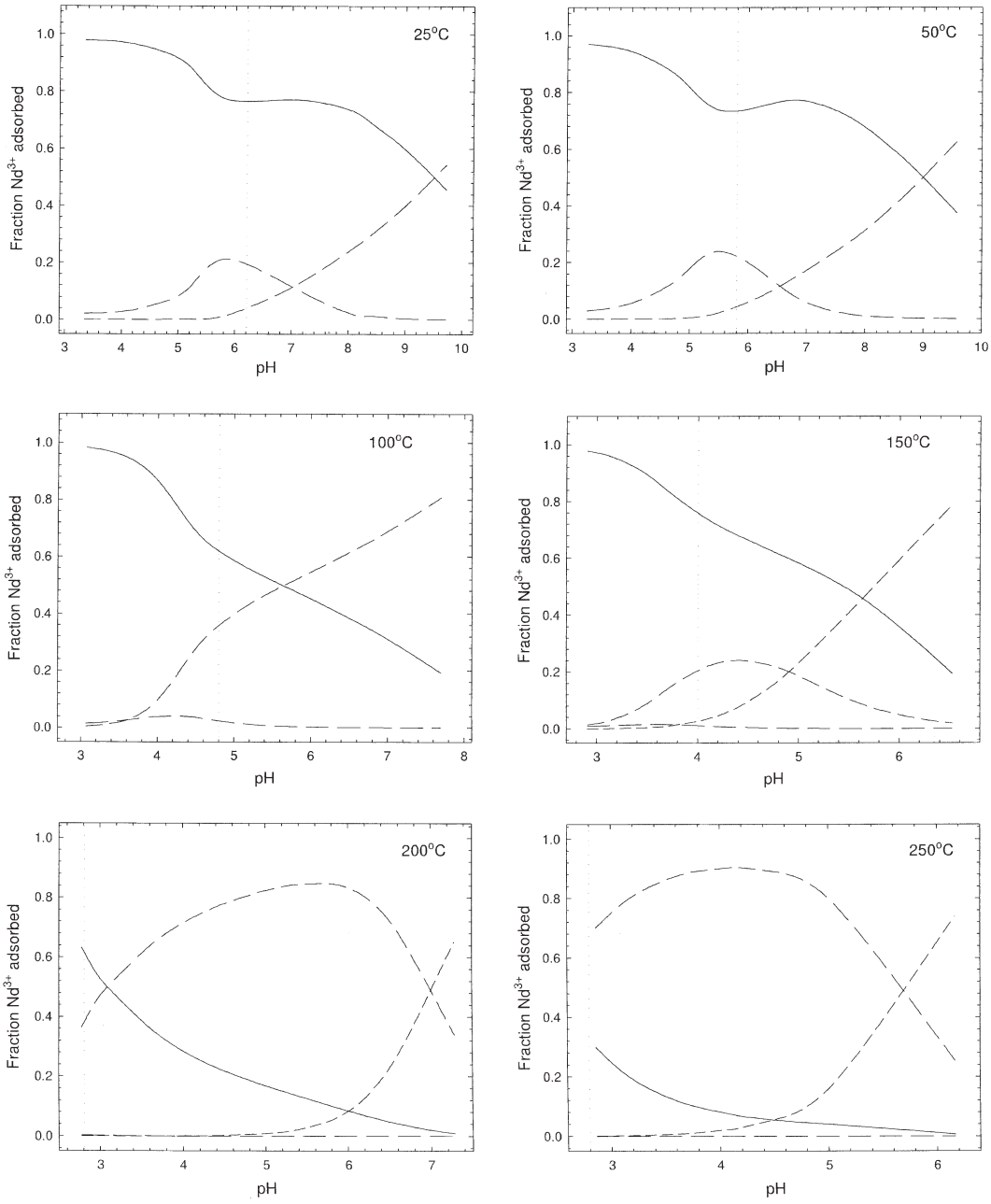

Fig. 8. The speciation of Nd presented as a fraction of the total Nd^{3+} adsorbed to rutile at 0.3*m* NaCl, plotted as a function of pH. The curves represent the fraction of TET-Nd (solid line), TET-NdOH (long dashed line), TET-$Nd(OH)_2$ (medium dashed line), and TET-$Nd(OH)_3$ (short dashed line). The dotted vertical lines represent the pH values where Nd^{3+} adsorption is virtually complete at each temperature.

5. RESULTS AND DISCUSSION

5.1. Model Fits

Experimental data (shown throughout as filled symbols) and best-fit curves (lines) for the sorption of Nd^{3+} onto rutile in a tetradentate configuration are shown in Figure 7, and the associated variable parameter, SD and MSC values are presented in Table 3. The net proton charge curves were fit significantly better when allowing for hydrolysis of adsorbed Nd^{3+}. This is demonstrated in Figure 7 columns A and B, which compare fits without and with the inclusion of adsorbed Nd^{3+} hydrolysis species, respectively. Fit improvement is especially noticeable above 50°C where, for example, the MSC value increases from 4.35 to 5.7 at 150°C (Table 3). It was possible to improve the fits somewhat without hydrolysis by allowing for larger inner Stern layer capacitance values (C_1), but this improved the fit only at low pH values where the Nd^{3+} was incompletely adsorbed (as indicated by the abrupt change in slope at temperatures ≤150°C in Fig. 7). The poorest fit is at 250°C and in this instance, the 0.30*m* titration data are suspect. First, the

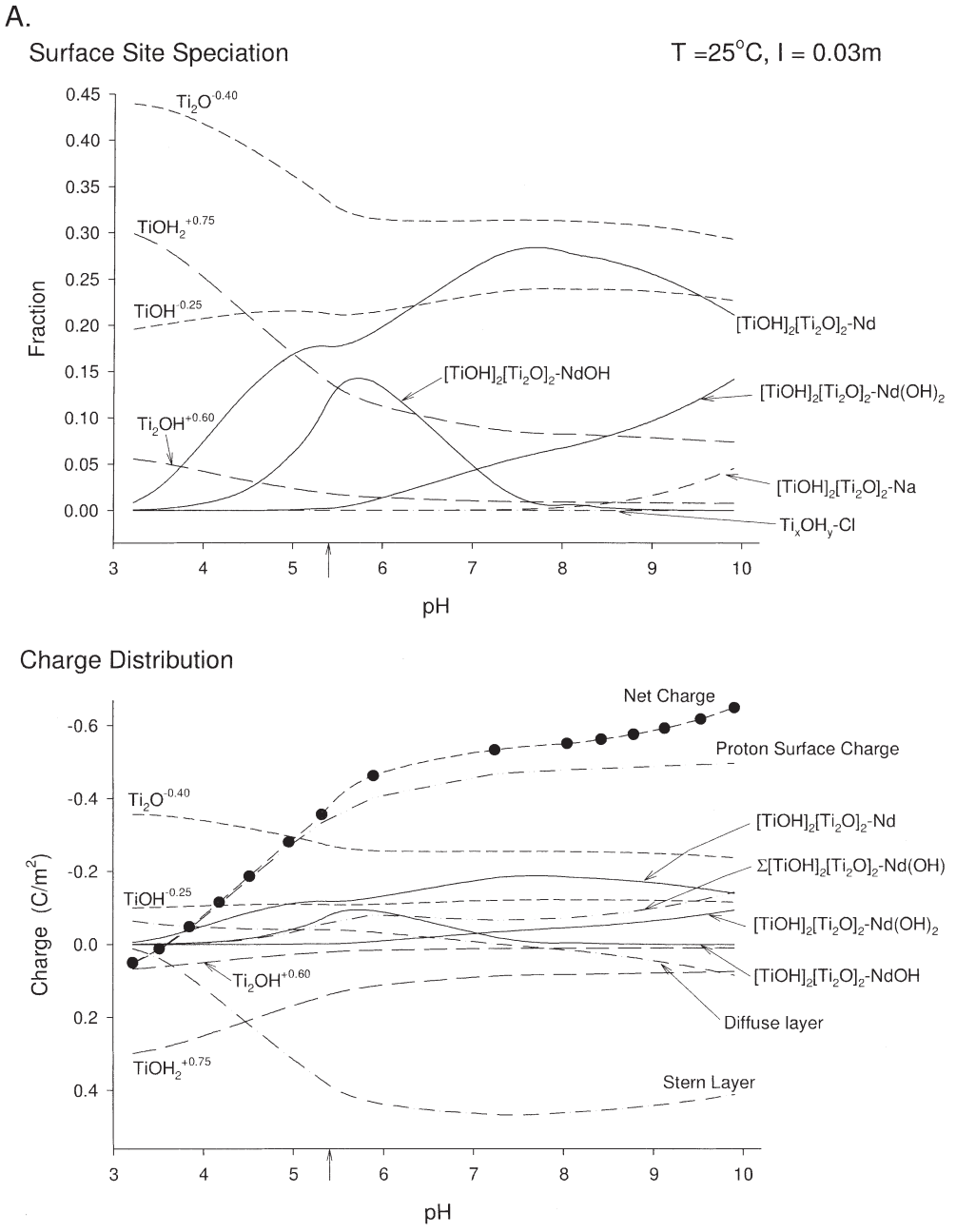

Fig. 9. Distribution of surface species at A. 25°C and I = 0.03*m* and B. 150°C and I = 0.3*m* with 0.001*m* initial Nd^{3+}. In the upper plots surface species are presented as fractions of the total concentration of surface sites, $N_{S,}$ which was fixed at 20.8 μmol/m^2. The lower plots show the charge contribution of each surface species to the total proton induced surface charge. The arrows at pH 5.4 and 4.4 indicate the pH_{znpc} value at 25 and 150°C, respectively

ionic strength dependence of the charge curves is much greater at 250°C than at the other temperatures, and second, the net 0.30*m* NaCl proton charge curve at 200°C is actually somewhat higher than that at 250°C which is opposite to the expected trend. Consequently, the 0.30*m* data were not considered in arriving at the 250°C model parameters in Table 3. All adsorption constants increase with temperature (consistent with increasing Nd^{3+} adsorption with temperature) and associated standard deviations are generally less than 5% of the adsorption constant values themselves except for log $K_{TET\text{-}NdOH}$ at 100 and 150°C where the SD values are ~30% of the fitted values. In this instance the large SD values result because the $[(\equiv TiOH^{-0.254})_2(\equiv Ti_2O^{-0.405})_2\text{–}NdOH^{2+}]$ species is a very minor contributor to the fitted total adsorbed Nd^{3+} concentration at temperatures ≥100°C (Fig. 8). In fact, log $K_{TET\text{-}Nd}$ and log $K_{TET\text{-}NdOH}$ values at 200 and 250°C were estimated, based on fits (Eqn. 26 below) to the corresponding fitted lower temperature values. Otherwise, given the small concentration of these species, fitted values were accompanied by SD values many times larger than the values themselves.

B.

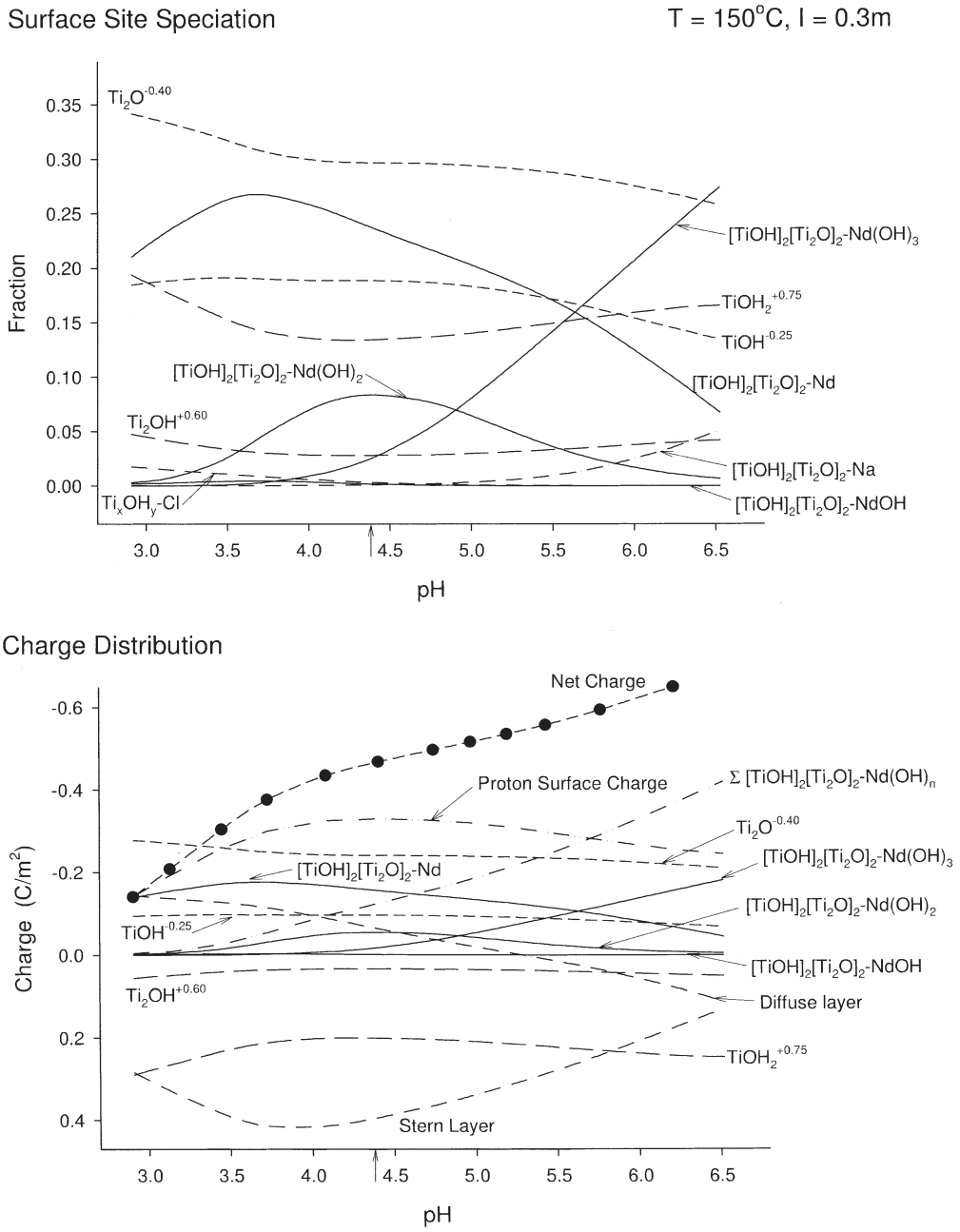

Fig. 9. (continued)

Justification for the hydrolysis of adsorbed Nd^{3+} (in terms of significantly improved model fits) rests largely on those portions of net proton charge curves where Nd^{3+} adsorption was virtually complete; at 200 and 250°C this occurred very near the start of the titrations. This is illustrated in Figure 8, which presents the fractional distribution of adsorbed Nd^{3+} species in 0.3*m* NaCl at each temperature, with the vertical line signifying the pH value where Nd^{3+} is ≥98% adsorbed. As temperature increases at a given pH value, both the extent and degree to which adsorbed Nd^{3+} is hydrolyzed increases. For example, at 25°C adsorbed Nd^{3+} hydrolysis exceeds 10% of the total Nd^{3+} adsorbed only above pH 5, with $NdOH^{2+}$ and then $Nd(OH)_2{}^{+}$ predominating as pH increases. At 150°C adsorbed Nd^{3+} hydrolysis species exceed 10% of the total Nd^{3+} adsorbed above pH 3.6 with $Nd(OH)_2{}^{+}$ and then $Nd(OH)_3{}^{\circ}$ dominant above pH 4.8. Undoubtedly, invoking adsorbed Nd^{3+} hydrolysis would not have been justified had only lower temperature data (≤50°C) been available. Moreover, net proton charge data in the pH range where Nd^{3+} is essentially completely adsorbed benefited most from the inclusion of hydrolysis. Similar data

have seldom been collected in other cation adsorption studies, which have tended to focus on adsorption pH-edge or constant-pH adsorption isotherm data, but such data are not useful for modeling purposes above pH values of essentially complete cation adsorption.

The hydrolysis of adsorbed cations is a common surface complexation model construct, especially for trivalent cations (e.g., James and Healy, 1972; Dzombak and Morel, 1990; Stumm, 1992). Trivalent cation hydrolysis is also consistent with some pressure-jump kinetic data (Lin et al., 1997). Hiemstra and van Riemsdijk (2002) propose that adsorbed cations are either more or less prone to hydrolysis depending on the degree of distortion of their coordination environment relative to homogeneous solutions. They argue that shorter bond lengths between the cation and surface oxygen atoms tend to lengthen cation-water bond lengths, and hence suppress hydrolysis (and vice versa). Moreover, if the surface oxygen atoms are bonded to a proton, sufficiently short cation-surface oxygen bonds can result in the deprotonation of these surface oxygens, which in terms of macroscopic net proton charge data would be virtually indistinguishable from adsorbed cation hydrolysis as a source of protons. On rutile, potential sources of such protons are the terminal surface oxygens (Eqn. 1). Bond lengths between Y^{3+} and surface oxygens on the rutile (110) surface are ~2.6 and 2.4 Å to the bridged and terminal oxygens, respectively, as determined from the X-ray standing wave experiments of Zhang et al. (2004). The average of these bond lengths is slightly longer than those to Y^{3+} in bulk solution (2.37 Å; Marcus, 1988). Bulk solution Nd^{3+}-oxygen bond lengths are slightly longer (2.47 Å; Marcus, 1988), but by analogy to adsorbed Y^{3+}, it is expected that adsorbed Nd^{3+}-surface oxygen bond lengths would be similar to or possibly slightly longer than those in bulk solution. Consequently, surface hydrolysis of adsorbed Nd^{3+} is a more likely source of protons than deprotonation of terminal oxygens. Also, Nd^{3+} is known to coordinate to nine water molecules in bulk solution in a tricapped-trigonal prism arrangement (Richens, 1997; D'Angelo et al., 2001). Consequently, even in a tetrahedral coordination with surface oxygen atoms and including interaction with the three-coordinated oxygen in the Ti-O surface plane, which directly underlies the cation sorbed in the tetradentate site, there are up to four additional hydration water molecules remaining that could potentially hydrolyze. Moreover, given that these water molecules are up to 2.5 Å higher above the surface than Nd^{3+}, the electrostatic gradient experienced by a leaving proton would be less than that applicable to Nd^{3+} itself. Consequently, in our modeling approach for adsorbed Nd^{3+} hydrolysis (Eqns. 11–13) it was assumed that the leaving protons originated at the outer Stern plane, on average, and therefore experienced an electrostatic gradient equal to that of Na^+ and Cl^- at the head of the diffuse layer (Fig. 6).

There is some in situ spectroscopic evidence for the formation of hydrolyzed and multinuclear cation adsorption complexes at higher surface coverage on rutile near room temperature. The XAFS results of O'Day et al. (1996) for Co^{2+} adsorption on rutile powders suggest multinuclear Co^{2+} complexes were formed at surface coverages >1.5 μmols/m^2 and pH values between 5.3 and 7.9. Similarly, Towle et al. (1999a) found evidence for multinuclear and partially hydrolyzed Co^{2+} adsorption complexes on single crystal rutile 110 and 001 surfaces at pH >7 and surface coverages of ~10 μmols/m^2. However, Zhang et al. (2004) found no evidence for significant Y^{3+} multinuclear species or surface precipitation on rutile (110) from their X-ray standing wave experiments, but these measurements were insensitive to surface hydrolysis. Moreover, these measurements were conducted only at room temperature and pH 6.1, and under these conditions Nd^{3+} modeling results suggest that adsorbed Nd^{3+} (and by inference adsorbed Y^{3+}) is predominately unhydrolyzed (Fig. 8). Regardless, direct spectroscopic confirmation of adsorbed Nd^{3+} hydrolysis is lacking at present.

5.2. Surface Speciation and EDL Charge Distribution

Surface-site speciation and the associated distribution of charge between the various surface groups and EDL planes are presented in Figure 9 for 0.03*m* NaCl at 25°C and 0.30*m* NaCl at 150°C as representative examples. The dominant positive and negative surface sites are Ti-$OH_2^{+0.746}$ and Ti_2-$O^{-0.405}$, respectively, with the latter decreasing in abundance as pH increases due to binding with Nd^{3+} and Na^+. However, Nd^{3+} is primarily responsible for the decrease since counterion binding (Na^+, Cl^-) is relatively minor (≤5% coverage) over the entire titration pH range. Given a total surface site concentration of 20.8 μmol/m^2, and tetradentate coordination, maximum Nd^{3+} surface coverage is ~40% of the available sites for our experimental conditions. Adsorbed Nd^{3+} is predominately unhydrolyzed over the entire pH range at 25°C, but at 150°C unhydrolyzed Nd^{3+} only predominates at pH <5.5.

The charge distribution plots in Figure 9 illustrate how the measured net proton charge is partitioned between contributions from the proton-only surface charge (σ_{PS}, Eqn. 17) and adsorbed Nd^{3+} hydrolysis (σ_{Hydrol}, Eqn. 24), as well as between the surface (σ_{PS}, Eqn. 17), inner Stern (σ_{Nd}, Eqn. 18) and diffuse (σ_d, Eqn. 22) layers. Net charge is dominated by the σ_{PS} contribution over the entire pH range at 25°C, but only below pH 5.5 at 150°C, which is a direct reflection of the increasing dominance of adsorbed Nd^{3+} hydrolysis with increasing temperature. However, total charge at the inner Stern layer actually decreases with the increasing dominance of hydrolyzed surface Nd species because of their lower charge. Consequently, the improved model fits resulting from the inclusion of hydrolysis (Fig. 7) result primarily from a balance between two competing effects. That is, the increase in proton release accompanying hydrolysis, and the diminished electrostatic or charge compensation proton contribution of the lower charged hydrolyzed species adsorbed at the inner Stern layer.

5.3. Temperature Dependence

All best-fit Nd adsorption constants increase systematically with temperature as anticipated by analogy to increased ion association in solution with increasing temperature (Mesmer et al., 1988). This increase is illustrated in Figure 10, where the lines associated with $\log K_{TET\text{-}Nd}$, $\log K_{TET\text{-}NdOH,}$ and $\log K_{TET\text{-}Nd(OH)2}$ represent fits using the equation (Murray and Cobble, 1980),

$$\log\ K_T = -[\Delta H^\circ_{298} - 298\Delta C_p/2.303R]\ T^{-1} + [\Delta S^\circ_{298} - \Delta C_p(1 + \ln 298)/2.303R] + (\Delta C_p/R)\log T \quad (26)$$

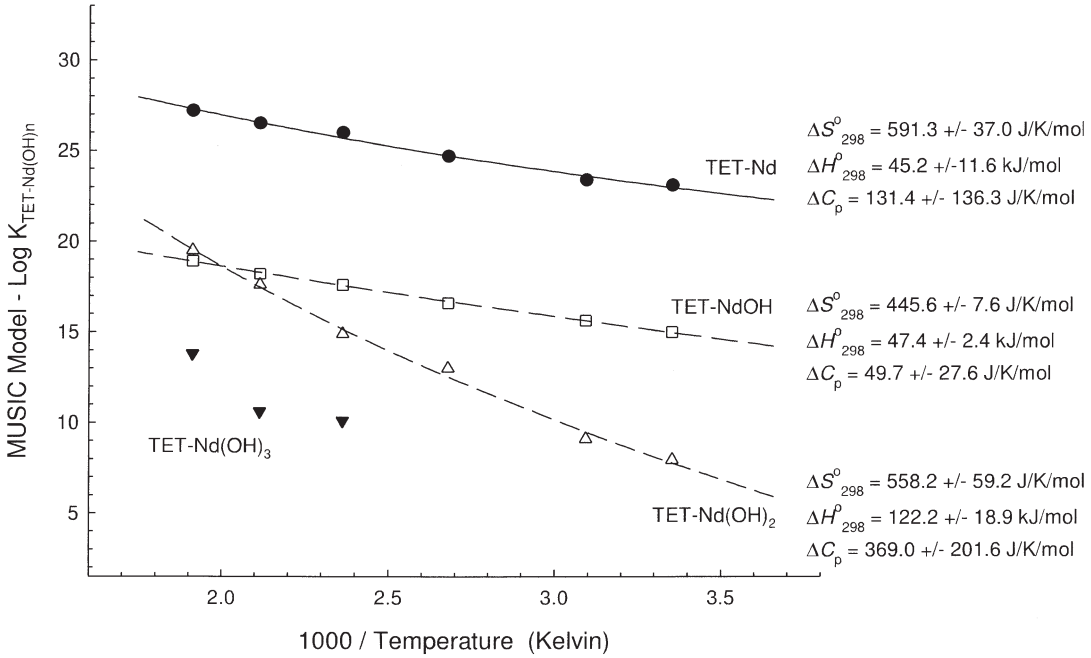

Fig. 10. Binding constants for the adsorption of Nd^{3+} on to rutile in a tetradentate configuration ($\log K_{TET\text{-}Nd}$) and the hydrolysis of adsorbed Nd ($\log K_{TET\text{-}Nd(OH)n}$) are presented as a function of the reciprocal temperature in Kelvin. The curves represent fits of Eqn. 26 for $\log K_{TET\text{-}Nd}$, $\log K_{TET\text{-}NdOH}$, and $\log K_{TET\text{-}Nd(OH)2}$, and the corresponding best-fit thermodynamic quantities are presented.

where T is temperature in Kelvin and ΔH°_{298}, ΔS°_{298} and ΔC_P are the standard enthalpy, entropy and heat capacity changes associated with the adsorption of Nd species onto rutile; and ΔC_P is assumed to be independent of temperature. The best-fit values of these thermodynamic quantities are given in Figure 10 ($\log K_{TET\text{-}Nd(OH)3}$ has been omitted from this analysis because best-fit constants are only available at three temperatures). Note that the standard deviations of the ΔC_P values are rather large (>50% of the values themselves) which indicates that a two-term fit (ΔH°_{298}, ΔS°_{298} only) would be nearly as good. In any case, these adsorption reactions are all endothermic at 25°C and are driven by large entropy terms as is typical of homogeneous ion association reactions in general. A dominant entropic contribution was also found for the adsorption of Ca^{2+} by rutile over the same temperature range (Ridley et al., 2004).

Previous investigations have noted that the adsorption constants of metal cations are linearly correlated with the corresponding aqueous hydrolysis constants at room temperature (e.g., Dzombak and Morel, 1990; Kosmulski, 1997b; Lin et al., 1997). The recent experimental studies of aqueous Nd^{3+} hydrolysis conducted by Klungness and Byrne (2000) also allow us to examine the degree of correlation between surface and solution Nd^{3+} hydrolysis for the first hydrolysis constant at 25 and 50°C. Subtracting the reverse of Eqn. 4 from Eqn. 5 results in,

$$[(\equiv TiOH^{-0.254})_2(\equiv Ti_2O^{-0.405})_2] - Nd^{3+} + H_2O = [(\equiv TiOH^{-0.254})_2(\equiv Ti_2O^{-0.405})_2] - NdOH^{2+} + H^+ \quad (27)$$

which is of the same form as the corresponding solution first hydrolysis constant. First hydrolysis constants (log values) for the surface reaction are −8.1 and −7.8 at 25 and 50°C, respectively, while the corresponding first hydrolysis reactions in solution are very similar (−8.2 and −7.4, respectively), in agreement with the linear correlation found for other cations in previous studies. It is not possible to reliably examine the first hydrolysis correlation at temperatures above 50°C, since both this study and the solution hydrolysis study of Wood et al. (2002) indicate a negligible or small predominance field for $NdOH^{2+}$ in pH space at temperatures ≤250°C. However, the $Nd(OH)_3^\circ$ species has a considerable predominance region at 250°C both on the surface and in solution. In this instance the surface hydrolysis constant (Eqn. 7 minus the reverse of Eqn. 4) is −13.4 while the corresponding solution value interpolated from the results of Wood et al. (2002) is considerably less (−15.7).

6. CONCLUSIONS

The potentiometric titration results presented here show that Nd^{3+} sorbs strongly to the rutile surface at all temperatures (25 to 250°C) and ionic strengths (0.03 and 0.3*m*) studied. Moreover, the adsorption of Nd^{3+} onto rutile commences well below the pH_{znpc} and shows little ionic strength dependence. Neodymium adsorption increases systematically with increasing temperature, but the stoichiometric proton release (moles H^+ released / moles Nd^{3+} adsorbed) remains fairly constant with increasing temperature.

The Nd^{3+} adsorption data overall were successfully described by explicit consideration of an inner-sphere tetradentate adsorption complex, (by analogy to that identified for Y^{3+} by X-ray standing wave measurements) within a surface-complexation model employing the MUSIC model approach and a Stern-based three-layer description of the EDL structure. Ad-

sorbed Nd^{3+} was permitted to hydrolyze, which significantly improved model fits especially above 50°C and at higher pH values. The quality of the model fits was highest from 25 to 150°C, with the poorer fits at 200 and 250°C at least partly resulting from Nd^{3+} being nearly completely adsorbed when the titrations commenced at these temperatures. The increased Nd^{3+} adsorption with increasing temperature is reflected by the systematic increase in best-fit nonhydrolyzed and hydrolyzed tetradentate binding constants, while the associated inner Stern layer capacitance values were relatively constant (5.0 to 6.6). Although the Nd^{3+} adsorption data were fitted successfully with a single tetradentate configuration and the permitted hydrolysis, we cannot exclude the possibility that some alternate surface complexes and/or hydrolysis products (e.g., Nd-OH-Cl, multinuclear complexes) may also exist. This is the first time that trivalent cation adsorption has been studied and modeled well into the hydrothermal regime. Specifically, this is the first use of any surface complexation model coupled with molecular-scale X-ray or spectroscopic information to uniquely describe trivalent cation adsorption beyond room temperatures. This study demonstrates that it is possible to develop conceptual models for multivalent ion adsorption over wide temperature ranges that are mechanistically accurate and thermodynamically rigorous.

Acknowledgments—This research was support by the National Science Foundation (EAR-0124001 and EAR-9627784) and by the Office of Basic Energy Sciences, U.S. Department of Energy, under contract DE-AC05-00OR22725 with Oak Ridge National Laboratory, managed by UT-Battelle, LLC. MLM acknowledges the support of the Illinois State Water Survey and the Illinois Department of Natural Resources. Jonathan Talbott of the Illinois Waste Management and Research Center conducted the ICP-MS analyses for total dissolved Nd.

Associate editor: D. Sverjensky

REFERENCES

Akaike H. (1976) An information criterion (AIC). *Math Sci.* **14,** 5–9.

Archer D. G. and Wang P. (1990) The dielectric-constant of water and Debye-Huckel limiting law slopes. *J. Phys. Chem. Ref. Data* **19,** 371–411.

Ardizzone S., Formaro L., and Lyklema J. (1981) Adsorption from mixtures containing mono- and bivalent cations on insoluble oxides and a revision of the interpretation of points of zero charge obtained by titration. *J. Electroanal. Chem.* **133,** 147–156.

Bandura A. V. and Kubicki J. D. (2003) Derivation of force field parameters for TiO_2-H_2O systems from ab initio calculations. *J. Phys. Chem. B.* **107,** 11072–11081.

Bedzyk M. J. and Cheng L. (2002) X-ray standing wave studies of minerals and mineral surfaces: Principles and applications. In *Applications of Synchrotron Radiation in Low-Temperature Geochemistry and Environmental Science* (eds. P. A. Fenter, M. L. Rivers, N. C. Sturchio and S. R. Sutton), pp. 221–266. Reviews in Mineralogy 49. Mineralogical Society of America.

Boily J. F. (1999) The surface complexation of ions at the qoethite α-FeOOH/wata interface. A multisite complexation approach. Ph.D. *Thesis.* Umea University, Umea, Sweden

Brown G. E. Jr., Henrich V. E., Casey W. H., Clark D. L., Eggleston C., Felmy A., Goodman D. W., Gratzel M., Maciel G., McCarthy M. I., and Nealson K. H. (1999) Metal oxide surfaces and their interactions with aqueous solutions and microbial organisms. *Chem. Rev.*, **99,** 77–174.

Criscenti L. J. and Sverjensky D. A. (2002) A single-site model for divalent transition and heavy metal adsorption over a range of metal concentrations. *J. Colloid Inter. Sci.* **253,** 329–352.

D'Angelo P., Pavel N. V., and Borowski M. (2001) K- and L-edge determination of the local structure of aqueous Nd(III) and Eu(III). *J. Synchroton Rad.* **8,** 666–668.

Davis J. A. and Kent D. B. (1990) Surface complexation modeling in aqueous geochemistry. In *Mineral-Water Interface Geochemistry* (eds. M. F. Hochella Jr. and A. F. White), pp. 281–307. Reviews in Mineralogy 23. Mineralogical Society of America.

Dzombak D. A. and Morel F. M. M. (1990) *Surface Complexation Modeling-Hydrous Ferric Oxide.* Wiley.

Fenter P., Cheng L., Rihs S., Machesky M., Bedzyk M. J., and Sturchio N. C. (2000) Electrical double-layer structure at the rutile-water interface as observed in situ with small-period x-ray standing waves. *J. Colloid Inter. Sci.* **225,** 154–165.

Fokkink L. G. J., De Keizer A., and Lyklema J. (1987) Specific adsorption on oxides: Surface charge adjustment and proton stoichiometry. *J. Colloid Inter. Sci.* **118,** 454–462.

Fokkink L. G. J., De Keizer A., and Lyklema J. (1990) Temperature dependence of cadmium adsorption on oxides. I. Experimental observations and model analysis. *J. Colloid Inter. Sci.* **135,** 118–131.

Gibb A. W. M. and Koopal L. K. (1990) Electochemistry of a model for patchwise heterogeneous surfaces: The rutile-hematite system. *J. Colloid Inter. Sci.* **134,** 12–138.

Hayes K. F. and Katz L. E. (1996) Application of x-ray absorption spectroscopy for surface complexation modeling of metal ion adsorption. In *Physics and Chemistry of Mineral Surfaces* (ed. P. V. Brady), pp. 147–223. CRC Press.

Helgeson H. C. (1969) Thermodynamics of hydrothermal systems at elevated temperatures and pressures. *Am. J. Sci.* **267,** 729–804.

Helgeson H. C., Kirkham D. H., and Flowers G. C. (1981) Theoretical prediction of the thermodynamic behavior of aqueous-electrolytes at high-pressures and temperatures. 4. Calculation of activity-coefficients, osmotic coefficients and apparent molal and standard and relative partial molal properties to 600-degrees-C and 5 Kb. *Am. J. Sci.* **281,** 1249–1516.

Hiemstra T., van Riemsdijk W. H., and Bolt G. H. (1989) Multisite proton adsorption modeling at the solid/solution interface of (hydr)oxides: A new approach *J. Colloid Interface Sci.* **133,** 91–104.

Hiemstra T. and van Riemsdijk W. H. (1991) Physical-chemical interpretation of primary charging behavior of metal (hydr)oxides. *Colloids Surf.* **59,** 7–25.

Hiemstra T., Venema P., and Van Riemsdijk W. H. (1996) Intrinsic proton affinity of reactive surface groups of metal (Hydr)oxides: The bond valence principle. *J. Colloid Interface Sci.* **184,** 680–692.

Hiemstra T. and van Riemsdijk W. H. (2002) On the relationship between surface structure and ion complexation of oxide-solution interfaces. In *Encyclopedia of Colloid and Interface Science* (ed. A. T. Hubbard), pp. 3773–3799. Marcel Dekker.

Ho P., Palmer D. A., and Mesmer R. E. (1994) Electrical conductivity measurements of aqueous sodium chloride solutions to 600°C and 300 MPa. *J. Solution Chem.* **23,** 997–1018.

Hohl H. and Stumm W. (1976) Interaction of Pb^{2+} with hydrous g-Al_2O_3. *J. Colloid Interface Sci.* **55,** 281–288.

James R. O. and Healy T. W. (1972) Adsorption of hydrolysable metal ions at the oxide-water interface. III. Thermodynamic model of adsorption. *J. Colloid Interface Sci.* **40,** 65–81.

Jang H. M. and Fuerstenau D. W. (1986) The specific adsorption of alkaline-earth cations at the rutile/water interface. *Colloids Surf.* **21,** 235–257.

Jones P. and Hockey J. A. (1971) Infra-red studies of rutile surfaces. 2. Hydroxylation, hydration and structure of rutile surfaces. *Trans. Faraday Soc.*, **67,** 2679–2685.

Klungness G. D. and Byrne R. H. (2000) Comparative hydrolysis behavior of the rare earths and yttrium: The influence of temperature and ionic strength. *Polyhedron* **19,** 99–107.

Kosmulski M. (1996) Adsorption of cadmium on alumina and silica: Analysis of the values of stability constants of surface complexes calculated for different parameters of triple layer model. *Colloids Surf.* **117,** 201–214.

Kosmulski M. (1997a) Standard enthalpies of adsorption of di- and trivalent cations on alumina. *J. Colloid Interface Sci.* **192,** 215–227.

Kosmulski M. (1997b) Adsorption of trivalent cations on silica. *J. Colloid Interface Sci.* **195,** 395–403.

Kosmulski M. (1999) Adsorption of trivalent cations on silica. II. Temperature effect. *J. Colloid Interface Sci.* **211,** 410–412.

Lin C-F., Chang K-S., Tsay C-W., Lee D-Y., Lo S-L., and Yasunaga T. (1997) Adsorption mechanism of gallium(III) and indium(III) onto γ-Al_2O_3. *J. Colloid Interface Sci.* **188,** 201–208.

Machesky M. L., Palmer D. A., and Wesolowski D. J. (1994) Hydrogen ion adsorption at the rutile-water interface to 250°C. *Geochim. Cosmochim. Acta* **58,** 5627–5632.

Machesky M. L., Wesolowski D. J., Palmer D. A., and Hayashi K. I. (1998) Potentiometric titrations of rutile suspensions to 250°C. *J. Colloid Interface Sci.* **200,** 298–309.

Machesky M. L., Wesolowski D. J., Palmer D. A., and Ridley M. K. (2001) On the temperature dependence of intrinsic surface protonation equilibrium constants: An extension of the revised MUSIC model. *J. Colloid Interface Sci.* **239,** 314–327.

Marcus Y. (1988) Ionic radii in aqueous solutions. *Chem. Rev.* **88,** 1475–1498.

Meissner H. P. and Kusik C. L. (1972) Activity coefficients of strong electrolytes in multicomponent aqueous solutions. *AIChE J.* **18,** 294–298.

Mesmer R. E., Marshall W. L., Palmer D. A., Simonson J. M., and Holmes H. F. (1988) Thermodynamics of aqueous association and ionization reactions at high-temperatures and pressures. *J. Sol. Chem.* **17,** 699–718.

Migdisov A. A. and Williams-Jones A. E. (2002) A spectrophotometric study of neodymium (III) complexation in chloride solutions. *Geochim. Cosmochim. Acta* **66,** 4311–4323.

Murray R. C. and Cobble J. W. (1980) Chemical equilibria in aqueous systems at high temperatures. In *Proceedings of the 41st International Water Conference*, pp. 1–82. Eng. Soc. Western PA.

O'Day P. A., Chisholm-Brause C. J., Towle S. N., Parks G. A., and Brown G. E. Jr. (1996) X-ray absorption spectroscopy of Co(II) sorption complexes on quartz (α-SiO_2) and rutile (TiO_2). *Geochim. Cosmochim. Acta* **60,** 2515–2532.

Palmer D. A. and Drummond S. E. (1988) Potentiometric determination of the molal formation constants of ferrous acetate complexes in aqueous solution to high temperatures. *J. Phys. Chem.* **92,** 6795–6800.

Palmer D. A. and Wesolowski D. J. (1993) Aluminum speciation and equilibria in aqueous solution: III. Potentiometric determination of the first hydrolysis constant of aluminum(III) in sodium chloride solutions to 125°C. *Geochim. Cosmochim. Acta* **57,** 2929–2938.

Pitzer K. S., Peiper J. C., and Busey R. H. (1984) Thermodynamic properties of aqueous sodium-chloride solutions. *J. Phys. Chem. Ref. Data* **13,** 1–102.

Richens D. T. (1997) *The Chemistry of Aqua Ions.* Wiley-Interscience.

Ridley M. K., Palmer D. A., Wesolowski D. J., and Kettler R. M. (1998a) Potentiometric and solubility studies of association quotients of aluminum malonate complexation in NaCl media to 75°C. *Geochim. Cosmochim. Acta* **62,** 2279–2291.

Ridley M. K., Palmer D. A., Wesolowski D. J., and Kettler R. M. (1998b) Cadmium malonate complexation in aqueous sodium trifluoromethanesulfonate media to 75°C, including dissociation quotients of malonic acid. *J. Sol. Chem.* **27,** 195–216.

Ridley M. K., Machesky M. L., Wesolowski D. J., and Palmer D. A. (1999) Calcium adsorption at the rutile-water interface: A potentiometric study in NaCl media to 250°C. *Geochim. Cosmochim. Acta* **63,** 3087–3096.

Ridley M. K., Machesky M. L., Palmer D. A., and Wesolowski D. J. (2002) Potentiometric studies of the rutile-water interface: Hydrogen-electrode concentration-cell vs. glass-electrode titrations. *Colloids Surf. A Physicochem. Eng. Aspects* **204,** 295–308.

Ridley M. K., Machesky M. L., Wesolowski D. J., and Palmer D. A. (2004) Modeling the surface complexation of calcium at the rutile-water interface to 250°C. *Geochim. Cosmochim. Acta* **68,** 239–251.

Rietra R. P. J. J., Hiemstra T., and van Riemsdijk W. H. (2001) Interaction between calcium and phosphate adsorption on goethite. *Environ. Sci. Technol* **35,** 3369–3374.

Sverjensky D. A. (2001) Interpretation and prediction of triple-layer model capacitances and the structure of the oxide-electrolyte-water interface. *Geochim. Cosmochim. Acta* **65,** 3643–3655.

Stumm W. (1992) *Chemistry of the Solid-Water Interface.* Wiley-Interscience.

Towle S. N., Brown G. E. Jr., and Parks G. A. (1999a) Sorption of Co(II) on metal oxide surfaces. I. Identification of specific binding sites of Co(II) on (110) and (001) surfaces of TiO_2 (rutile) by grazing-incidence XAFS spectroscopy. *J. Colloid Interface Sci.* **217,** 299–311.

Towle S. N., Bargar J. R., Brown G. E. Jr., and Parks G. A. (1999b) Sorption of Co(II) on metal oxide surfaces. II. Identification of Co(II)(aq) adsorption sites on the (0001) and (102) surfaces of α-Al_2O_3 by grazing-incidence XAFS spectroscopy. *J. Colloid Interface Sci.* **217,** 312–321.

Venema P., Hiemstra T., and van Riemsdijk W. H. (1996) Multisite adsorption of cadmium on goethite. *J. Colloid Interface Sci.* **183,** 515–527.

Waychunas G. A. (2002) Grazing-incidence X-ray absorption and emission spectroscopy. In *Applications of Synchrotron Radiation in Low-Temperature Geochemistry and Environmental Science* (eds. P. A. Fenter, M. L. Rivers, N. C. Sturchio and S. R. Sutton), chap. 5. Mineralogical Society of America.

Westall J. and Hohl H. (1980) A comparison of electrostatic models for the oxide/solution interface. *Adv. Colloid Interface Sci.* **12,** 265–294.

Wood S. A., Wesolowski D. J., and Palmer D. A. (2000) The aqueous geochemistry of the rare earth elements IX: A potentiometric study of Nd^{3+} complexation with acetate in 0.1 molal NaCl solution from 25°C to 225°C. *Chem. Geol.* **167,** 231–253.

Wood S. A., Palmer D. A., Wesolowski D. J., and Bénézeth P. (2002) The aqueous geochemistry of the rare earth elements and yttrium. Part XI. The solubility of $Nd(OH)_3$ and hydrolysis of Nd^{3+} from 30 to 290°C at saturated water vapor pressure with in-situ pH_m measurement. In *Water-Rock Interactions, Ore Deposits and Environmental Geochemistry: A Tribute to David A. Crear* (eds. R. Hellmann and S. A. Wood), pp. 229–278. St. Louis, Mo.: Geochemical Society.

Zhang Z. Fenter P., Cheng L., Sturchio N. C., Bedzyk M. J., Předota M., Bandura A., Kubicki J., Lvov S. N., Cummings P. T., Chialvo A. A., Ridley M. K., Bénézeth P., Anovitz L., Palmer D. A., Machesky M. L., and Wesolowski D. J. (2004) Ion adsorption at the rutile-water interface: Linking molecular and macroscopic properties. *Langmuir* **20,** 4954–4969.

Appendix A. Summary of surface charge (σ_H) data for the adsorption of Nd^{3+} onto a rutile surface.

pH	σ_H (C/m^2)	pH	σ_H (C/m^2)	pH	σ_H (C/m^2)	pH	σ_H (C/m^2)
T = 25°C; I = 0.03*m*		T = 25°C; I = 0.3*m*		T = 50°C; I = 0.03*m*		T = 50°C; I = 0.3*m*	
3.216	0.0514	3.343	0.0663	3.138	0.0246	3.254	0.0374
3.511	0.0213	3.794	0.0080	3.412	−0.0191	3.636	−0.0266
3.848	−0.0297	4.186	−0.0638	3.713	−0.0828	4.070	−0.1198
4.180	−0.0967	4.670	−0.1657	4.041	−0.1645	4.559	−0.2372
4.515	−0.1731	5.209	−0.2855	4.376	−0.2548	4.943	−0.3223
4.953	−0.2806	5.835	−0.4000	4.721	−0.3425	5.462	−0.4116
5.319	−0.3640	7.000	−0.4931	5.080	−0.4144	6.180	−0.4725
5.895	−0.4554	7.997	−0.5498	5.483	−0.4623	6.876	−0.5153
7.246	−0.5324	8.368	−0.5745	5.858	−0.4864	7.613	−0.5620
8.049	−0.5706	8.790	−0.6034	6.254	−0.5065	8.119	−0.5994
8.431	−0.5901	9.167	−0.6308	6.864	−0.5365	8.634	−0.6376
8.792	−0.6094	9.475	−0.6561	7.470	−0.5670	9.058	−0.6738
9.135	−0.6278	9.730	−0.6768	8.173	−0.6027	9.570	−0.7184
9.538	−0.6486			8.744	−0.6338		
9.915	−0.6697			9.108	−0.6547		
T = 100°C; I = 0.03*m*		T = 100°C; I = 0.3*m*		T = 150°C; I = 0.03*m*		T = 150°C; I = 0.3*m*	
2.947	−0.0658	3.065	−0.0509	2.747	−0.2206	2.906	−0.1810
2.962	−0.0690	3.281	−0.1052	2.891	−0.2664	3.132	−0.2448
3.163	−0.1205	3.593	−0.1974	3.039	−0.3112	3.450	−0.3295
3.397	−0.1899	3.963	−0.3008	3.225	−0.3609	3.731	−0.3836
3.674	−0.2749	4.336	−0.3815	3.542	−0.4254	4.092	−0.4231
3.953	−0.3529	4.666	−0.4239	3.842	−0.4595	4.415	−0.4494
4.325	−0.4194	5.126	−0.4596	4.161	−0.4819	4.751	−0.4748
4.777	−0.4603	5.556	−0.4926	4.468	−0.4993	4.981	−0.4931
5.146	−0.4809	6.148	−0.5359	4.850	−0.5192	5.203	−0.5111
5.640	−0.5065	6.796	−0.5877	5.180	−0.5353	5.442	−0.5307
6.170	−0.5347	7.323	−0.6367	5.529	−0.5520	5.779	−0.5603
6.773	−0.5676	7.703	−0.6748	5.881	−0.5709	6.226	−0.6048
7.178	−0.5923			6.191	−0.5865	6.529	−0.6386
7.576	−0.6155			6.525	−0.6074		
8.013	−0.6437						
		T = 200°C; I = 0.3*m*		T = 250°C; I = 0.03*m*		T = 250°C; I = 0.3*m*	
		2.776	−0.3444	2.564	−0.4856	2.861	−0.3335
		2.972	−0.3588	2.579	−0.4774	3.071	−0.3261
		3.221	−0.3599	2.671	−0.4400	3.268	−0.3282
		3.627	−0.3824	2.759	−0.4400	3.491	−0.3285
		4.042	−0.4064	2.868	−0.4381	3.741	−0.3426
		4.445	−0.4350	3.019	−0.4364	4.134	−0.3675
		4.912	−0.4691	3.213	−0.4397	4.510	−0.4031
		5.324	−0.5046	3.503	−0.4501	5.013	−0.4565
		5.799	−0.5477	3.871	−0.4645	5.763	−0.5697
		6.154	−0.5849	4.191	−0.4781	6.170	−0.6385
		6.551	−0.6330	4.566	−0.4940		
		6.992	−0.6952	4.818	−0.5067		
		7.288	−0.7474	5.156	−0.5227		
				5.463	−0.5397		
				5.663	−0.5550		
				6.057	−0.5832		
				6.427	−0.6110		

Appendix B. Summary of Nd^{3+} adsorption data.

pH	ΣNd (*m*)	Measured m_{Nd3+}	pH	ΣNd (*m*)	Measured m_{Nd3+}
T = 25°C; I = 0.03*m*			T=25°C;I=0.3*m*		
3.249	0.000991	0.001012	3.360	0.000996	0.001006
3.577	0.000940	0.000871	3.895	0.000920	0.000726
3.985	0.000890	0.000703	4.358	0.000868	0.000520
4.396	0.000843	0.000460	4.846	0.000819	0.000326
4.811	0.000800	0.000290	5.377	0.000774	0.000130
5.301	0.000757	0.000111	6.080	0.000738	0.000010
5.864	0.000731	0.000016	6.820	0.000721	0.000001
6.465	0.000719	0.000002	7.502	0.000707	0.000000
6.893	0.000711	0.000001	8.162	0.000692	0.000000
7.659	0.000698	0.000000			
T = 50°C; I = 0.03*m*					
3.163	0.000991	0.000948			
3.423	0.000938	0.000818			
3.731	0.000887	0.000625			
4.057	0.000840	0.000454			
4.400	0.000799	0.000302			
4.802	0.000760	0.000120			
5.241	0.000735	0.000026			
5.761	0.000721	0.000003			
6.334	0.000711	0.000001			
6.764	0.000703	0.000000			
T = 100°C; I = 0.03*m*					
2.962	0.000992	0.000777			
8.013	0.000671	0.000001			
T = 150°C; I = 0.03*m*			T = 150°C; I = 0.3*m*		
2.772	0.000994	0.000450	2.932	0.000997	0.000439
2.902	0.000932	0.000336	3.210	0.000887	0.000247
3.075	0.000868	0.000219	3.533	0.000815	0.000117
3.361	0.000801	0.000094	3.957	0.000770	0.000016
3.740	0.000756	0.000018	4.366	0.000750	0.000003
4.265	0.000731	0.000002	4.790	0.000737	0.000000
4.697	0.000720	0.000001	5.544	0.000716	0.000000
5.191	0.000709	0.000000			
5.668	0.000701	0.000000			
			T = 200°C; I = 0.3*m*		
			2.972	0.000919	0.000093
			7.288	0.000627	0.000000
T = 250°C; I = 0.03*m*			T = 250°C; I = 0.3*m*		
2.579	0.001013	0.000023	3.071	0.000934	0.000095
6.427	0.000685	0.000000	6.170	0.000679	0.000000